A SPHERE IN A SECOND DEGREE POLYNOMIAL CREEPING FLOW PARALLEL TO A WALL

by L. PASOL

(*Laboratoire PMMH, École Supérieure de Physique et Chimie Industrielles,* 10 *rue Vauquelin*, 75005 *Paris, France*)

A. SELLIER

(*LadhyX, Ecole Polytechnique*, 91128 *Palaiseau Cédex, France*)

and F. FEUILLEBOIS†

(*Laboratoire PMMH, École Supérieure de Physique et Chimie Industrielles,* 10 *rue Vauquelin*, 75005 *Paris, France*)

[Received 1 April 2006. Revise 4 October 2006. Accepted 12 October 2006]

Summary

Comprehensive results are provided for the creeping flow around a spherical particle in a viscous fluid close to a plane wall, when the external velocity is parallel to the wall and varies as a second degree polynomial in the coordinates. By linearity of Stokes equations, the solution is a sum of flows for typical unperturbed flows: a pure shear flow, a 'modulated shear flow', for which the rate of shear varies linearly in the direction normal to the wall, and a quadratic flow. Solutions considered here use the bipolar coordinates technique. They complement the accurate results of Chaoui and Feuillebois (2003) for the pure shear flow. The solution of Goren and O'Neill (1971) for the quadratic flow is reconsidered and a new analytical solution is derived for the ambient modulated shear flow. The perturbed flow fields for these two cases are presented in detail and discussed. Results for the force and torque friction factors are provided with a 5×10^{-17} accuracy as a reference. For the quadratic flow, there is a force and a torque on a fixed sphere. A minimum value of the torque is found for a gap of about $0{\cdot}18a$, where a is the sphere radius. This minimum is interpreted in term of the corresponding flow structure. For the modulated shear flow, there is only a torque. The free motion of a sphere in an ambient quadratic flow is also determined.

1. Introduction

The motion of particles in a fluid flow along a wall is of fundamental importance for various small scale systems, in microhydrodynamics or microfluidics. Various applications are concerned, for example, particle analysis or separation in analytical chemistry by techniques such as the *field-flow fractionation* (**1**).

The problems considered in this article concern a spherical solid particle embedded in a viscous fluid in the vicinity of a plane wall. At small scales, the Reynolds number is usually low and Stokes

†Corresponding author ⟨feuillebois@pmmh.espci.fr⟩

Advance Access publication 20 November 2006. doi:10.1093/qjmam/hbl018

equations apply. It is known from solutions of these equations (**2**) that hydrodynamic interactions are long-ranged. Therefore at small scales wall effects become quite significant.

The problem of the creeping flow around a sphere close to a plane wall has been addressed in various articles. A survey of the literature can be found in (**3**) and a preceding article (**4**) which treats the cases of a translating and rotating sphere in a fluid at rest and of a sphere held fixed in a shear flow. The present article is concerned with the more general case where the ambient velocity, parallel to the plane wall, varies as a polynomial of second degree in the coordinates. Note that polynomial unperturbed velocities in the direction perpendicular to the wall were considered in (**5**), so that by linear combinations various three-dimensional polynomial flow fields may be obtained.

As for various applications, it will be noted below that the polynomial flow velocity in one direction also satisfies Navier–Stokes equations. Thus the unperturbed creeping flow around the sphere near a wall may be the local description of some flow field satisfying the Navier–Stokes equations on a larger scale. This polynomial ambient flow may also be understood as a Taylor expansion in the coordinates of any general flow field along the wall. A second-order expansion is quite sufficient for many practical applications.

Since Stokes equations are linear, any unperturbed flow field along a wall can be understood as the superposition of unperturbed flow fields in two perpendicular directions. It is therefore sufficient to consider a polynomial flow field in one direction. Also because of linearity, the problem for a general unperturbed flow field in one direction may be decomposed as a sum of problems for elementary unperturbed flow fields. As for a pure shear flow, results of (**4**) may be used. It will be shown that two other unperturbed flow fields have to be considered: a quadratic shear flow and a 'modulated shear flow' for which the rate of shear varies linearly in the direction of the vorticity. New analytical solutions in bipolar coordinates will be given for these problems.

The bipolar coordinates (BC), pioneered by Jeffery (**6**), have been used in numerous publications involving a sphere and a plane wall; see (**3**) for a review and a list of references. In particular, the case of a rotating sphere was solved in (**7**), the case of translating sphere in (**8**, **9**) and the case of a sphere held fixed in a pure shear flow and in a quadratic flow in (**10**). The BC method provides the solution as series in these coordinates. The number of terms in the series increases for decreasing gap between the sphere and the wall. It is usually believed that the BC become inappropriate when this gap becomes small compared with the sphere radius, since the coefficients in the series are solutions of an increasingly large linear system. However, as shown in (**11**), numerous coefficients in the series can be calculated with a fast iteration procedure. Following this idea, comprehensive results were obtained by Chaoui and Feuillebois (**4**) for the problems of a sphere translating and rotating along a wall in a fluid at rest and that of a sphere held fixed in a shear flow along a wall. Their results for the force and torque on the sphere, which are valid with a 10^{-16} accuracy for values of the gap between the sphere and the wall down to 2×10^{-6} sphere radius, were obtained by calculating a large number of terms in the series without excessive computer resources. For a freely moving sphere in a shear flow, they also calculated the sphere translational and rotational velocities with the same accuracy. In a similar way, the problem of a sphere held fixed in a quadratic flow solved by Goren and O'Neill (**10**) is reconsidered here in more detail. Moreover, a novel analytical solution is presented for a modulated shear flow. For these flow fields, the force and torque on the sphere are calculated with a 5×10^{-17} accuracy for a large domain of values of the sphere to wall spacing. Results for the perturbed flow field are provided as well. Note that when the sphere is in contact with the wall, the BC method is inappropriate. For this case, analytical solutions in tangent sphere coordinates were obtained for an unperturbed shear flow in (**12**) and for an unperturbed quadratic flow in (**10**).

An alternative method to solve Stokes flow problems involving spherical particles is the multipole expansion method, which starts with analytical developments and can accommodate many spherical particles as well as one or two plane boundaries. That method is compared with the present one for the case of a single sphere and one wall by Ekiel-Jeżewska and Wajnryb in a companion article (**13**).

The present results may also be used as a benchmark for numerical techniques.

Of course, high accuracy for the force and torque is not directly needed in comparison with experiments since the neglected fluid inertia would contribute terms of order $O(\mathrm{Re})$, where Re is the Reynolds number which is usually larger than the present accuracy. On the other hand, accurate Stokes flow results are needed to calculate the second-order $O(\mathrm{Re})$ effects for a sphere in the vicinity of the wall. Work on this problem is in progress. Other second-order effects (**14**) may also be calculated on the basis of the present results.

The article is organized as follows. In section 2, we present the problems under consideration and introduce the notation and definitions of friction factors for the force and torque on the sphere. The analytical BC solution for the presented problems is derived in section 3. The results for a sphere held fixed or freely suspended in a quadratic or in a modulated ambient shear flow are presented and discused in section 4. We moreover provide interpolation formulae for the force and torque exerted on a sphere held fixed in a quadratic ambient shear flow. Finally, concluding remarks are presented in section 5.

2. Problems, notation and basic formulae

In this section we introduce the addressed problems and the notation, then define friction factors and mobilities.

Consider a sphere with radius a embedded in a semi-infinite region bounded by a plane wall. We use a system of Cartesian coordinates $Oxyz$ (with unit vectors $\boldsymbol{e}_x, \boldsymbol{e}_y, \boldsymbol{e}_z$) attached to the wall which is denoted by $z = 0$. The sphere may be moving and is centred on the z-axis at a distance ℓ from the wall at the time at which the flow field is observed. The unperturbed velocity field $\boldsymbol{u}_\infty$ is assumed to be along x, such that from continuity equation $\boldsymbol{u}_\infty = u_\infty(y, z)\,\boldsymbol{e}_x$. Its most general second-order expansion satisfying the creeping flow equations and the no-slip condition on the wall is

$$\boldsymbol{u}_\infty = (k_\mathrm{s} z + k_\mathrm{q} z^2 + 2k_\mathrm{m} z y)\,\boldsymbol{e}_x, \tag{1}$$

where $k_\mathrm{s}, k_\mathrm{q}, k_\mathrm{m}$ are constants. The only component with a non-constant pressure is the quadratic one, so that the unperturbed pressure p_∞ reads, up to an arbitrary constant,

$$p_\infty = 2\mu k_\mathrm{q} x. \tag{2}$$

More generally, note that (1) is also the most general second-order expansion of $\boldsymbol{u}_\infty$ parallel to x satisfying the Navier–Stokes equations. Then, as mentioned in the Introduction, various applications may be considered in which the flow far from the perturbed Stokes flow region may have a large Reynolds number based on some outer scale.

By linearity, the perturbed flow field $(\boldsymbol{u}_\infty + \boldsymbol{u},\ p_\infty + p)$ with unperturbed velocity and pressure given by (1) and (2) is calculated as the sum of solutions to three problems, with unperturbed velocity $k_\mathrm{s} z\,\boldsymbol{e}_x$ (pure shear flow), $k_\mathrm{q} z^2\,\boldsymbol{e}_x$ (quadratic flow) and $2k_\mathrm{m} z y\,\boldsymbol{e}_x$ (modulated shear flow), respectively. Results of (**4**) may be used for the pure shear flow. The case of a quadratic ambient flow is calculated here in a similar way and a new analytical solution is derived below for the

modulated shear flow. By linearity, the solution for the modulated shear flow may be written as the sum of those for two ambient flows:

$$2k_{\mathrm{m}} zy\, \boldsymbol{e}_x = k_{\mathrm{m}}(zy\, \boldsymbol{e}_x + zx\, \boldsymbol{e}_y) + k_{\mathrm{m}}(zy\, \boldsymbol{e}_x - zx\, \boldsymbol{e}_y).$$

The first contribution, that is a pure straining motion in each plane $z =$ constant, is called a 'modulated straining motion'. The second contribution, a rotational flow with vorticity varying along z, is called a 'modulated rotational flow'. Thus, we successively deal with a quadratic flow, a modulated straining motion and a modulated rotational flow.

The general problem considered here is that of a particle moving in this ambient flow field with given translational velocity $\boldsymbol{U}$ and rotational velocity $\boldsymbol{\Omega}$. This problem is solved by simply adding the cases of a translating and rotating sphere in a fluid at rest to that of a fixed sphere in the ambient flow field. For each separate case, the fluid applies on to the sphere a force $\boldsymbol{F}$ and a torque $\boldsymbol{C}$ which may be written in term of friction factors f and c (following notation of (**4**)) as

$$F_x^{\mathrm{t}} = -6\pi a \mu\, U\, f_{xx}^{\mathrm{t}} \qquad C_y^{\mathrm{t}} = 8\pi a^2 \mu\, U c_{yx}^{\mathrm{t}} \tag{3a}$$

$$F_x^{\mathrm{r}} = 6\pi a^2 \mu\, \Omega_y\, f_{xy}^{\mathrm{r}} \qquad C_y^{\mathrm{r}} = -8\pi a^3 \mu\, \Omega_y\, c_{yy}^{\mathrm{r}} \tag{3b}$$

$$F_x^{\mathrm{s}} = 6\pi a \ell \mu\, k_{\mathrm{s}}\, f_{xx}^{\mathrm{s}} \qquad C_y^{\mathrm{s}} = 4\pi a^3 \mu\, k_{\mathrm{s}} c_{yx}^{\mathrm{s}} \tag{3c}$$

$$F_x^{\mathrm{q}} = 6\pi a \ell^2 \mu\, k_{\mathrm{q}}\, f_{xx}^{\mathrm{q}} \qquad C_y^{\mathrm{q}} = 8\pi a^3 \ell \mu\, k_{\mathrm{q}} c_{yx}^{\mathrm{q}} \tag{3d}$$

$$C_z^{\mathrm{r}} = -8\pi a^3 \mu\, \Omega_z\, c_{zz}^{\mathrm{r}} \tag{3e}$$

$$C_z^{\mathrm{m}} = -8\pi a^3 \ell \mu\, k_{\mathrm{m}} c_{zx}^{\mathrm{m}}. \tag{3f}$$

The superscripts $()^{\mathrm{t}}$, $()^{\mathrm{r}}$, $()^{\mathrm{s}}$, $()^{\mathrm{q}}$, $()^{\mathrm{m}}$ denote the translation, rotation, shear flow, quadratic flow, modulated shear flow, respectively. The first subscript denotes the component of the force or torque and the second subscript indicates the direction of the unperturbed flow field. The results for the modulated shear flow are obtained by observing that it is the sum of a modulated straining motion giving zero force and torque and a modulated rotational flow giving a torque but no force. When ℓ becomes infinite, the friction factors c_{yx}^{t} and f_{xy}^{r} vanish and all other friction factors become unity, as can be checked by using Faxen formulae (**2**).

A freely moving sphere (that is, with zero total force and torque) embedded in an unperturbed flow field having shear and quadratic contributions moves with the following translational and rotational velocities:

$$U = k_{\mathrm{s}} a \tilde{U}^{\mathrm{s}} + k_{\mathrm{q}} a^2 \tilde{U}^{\mathrm{q}}, \tag{4a}$$

$$\Omega_y = k_{\mathrm{s}} \tilde{\Omega}_y^{\mathrm{s}} + k_{\mathrm{q}} a \tilde{\Omega}_y^{\mathrm{q}}, \tag{4b}$$

introducing the mobilities which, by (3) are obtained as

$$\tilde{U}^{\mathrm{s}} = \frac{(\ell/a) c_{yy}^{\mathrm{r}} f_{xx}^{\mathrm{s}} + \frac{1}{2} f_{xy}^{\mathrm{r}} c_{yx}^{\mathrm{s}}}{D}, \quad \tilde{\Omega}_y^{\mathrm{s}} = \frac{\frac{1}{2} f_{xx}^{\mathrm{t}} c_{yx}^{\mathrm{s}} + (\ell/a) c_{yx}^{\mathrm{t}} f_{yx}^{\mathrm{s}}}{D}, \tag{5a}$$

$$\tilde{U}^{\mathrm{q}} = \frac{(\ell/a)^2 c_{yy}^{\mathrm{r}} f_{xx}^{\mathrm{q}} + (\ell/a) f_{xy}^{\mathrm{r}} c_{yx}^{\mathrm{q}}}{D}, \quad \tilde{\Omega}_y^{\mathrm{q}} = \frac{(\ell/a) f_{xx}^{\mathrm{t}} c_{yx}^{\mathrm{q}} + (\ell/a)^2 c_{yx}^{\mathrm{t}} f_{xx}^{\mathrm{q}}}{D}, \tag{5b}$$

$$\text{where} \quad D = c_{yy}^{\mathrm{r}} f_{xx}^{\mathrm{t}} - f_{xy}^{\mathrm{r}} c_{yx}^{\mathrm{t}}. \tag{5c}$$

Consider first a freely moving sphere in a quadratic flow, that is, $k_s = 0$. The sphere translational and rotational velocities may be compared with those of a sphere embedded in the same unperturbed flow field, but in an *unbounded* fluid domain. From Faxen formulae, those velocities read $U_{un} = k_q(\ell^2 + a^2/3)$, $\Omega_{un} = k_q\ell$. It is therefore appropriate to introduce the normalized velocities

$$U^q = \frac{U}{U_{un}} = \frac{\tilde{U}^q}{(\ell/a)^2 + 1/3}, \tag{6a}$$

$$\Omega_y^q = \frac{\Omega_y}{\Omega_{un}} = \frac{\tilde{\Omega}_y^q}{(\ell/a)}, \tag{6b}$$

which tend to unity as $\ell/a \to \infty$.

3. Bipolar coordinates method and solutions

In the following, the BC method is used to solve the problems of the particle held fixed in the various components of the unperturbed flow field (1). The free motion of a sphere in a quadratic flow field is also calculated. The bipolar coordinates (ξ, η, ϕ) are related to the usual cylindrical polar coordinates (ρ, z, ϕ), with $x = \rho\cos\phi$ and $y = \rho\sin\phi$, as follows (**2**):

$$\rho = \frac{c\sin\eta}{\cosh\xi - \cos\eta}, \quad z = \frac{c\sinh\xi}{\cosh\xi - \cos\eta}, \quad c = (\ell^2 - a^2)^{1/2}. \tag{7}$$

The $z = 0$ plane corresponds to $\xi = 0$ whereas the $\xi = \alpha$ coordinate surface with $\ell = a\cosh\alpha$ is the surface $\mathcal{S}$ of the sphere. Accordingly, in the fluid domain we have $0 \leqslant \phi \leqslant 2\pi$, $0 \leqslant \eta \leqslant \pi$ and $0 \leqslant \xi \leqslant \alpha$. For convenience we shall also use the usual unit vectors $\mathbf{e}_\rho = (x\mathbf{e}_x + y\mathbf{e}_y)/\rho$ and $\mathbf{e}_\phi = \mathbf{e}_z \times \mathbf{e}_\rho$.

3.1 *Sphere held fixed in a quadratic flow and earlier similar problems*

The solution for the sphere held fixed in a quadratic flow is analogous to previous solutions for a translating or rotating sphere in a fluid at rest (**7** to **9**) and for a sphere held fixed in a shear flow (**10**). A general solution that includes all cases is presented here in uniform notation. The no-slip boundary condition on the sphere for the perturbation velocity in the four cases is respectively $\boldsymbol{u} = \boldsymbol{e}_x$ (translation), $\boldsymbol{u} = \boldsymbol{e}_y \times \boldsymbol{r}$ (rotation), $\boldsymbol{u} = -z\boldsymbol{e}_x$ (shear flow) and $\boldsymbol{u} = -z^2\boldsymbol{e}_x$ (quadratic flow). The general solution of the Stokes equations in the cylindrical coordinates system is of the form

$$u_\rho = \tfrac{1}{2}\{\rho Q_1 + U_0 + U_2\}\cos\phi, \quad u_\phi = \tfrac{1}{2}(U_2 - U_0)\sin\phi, \tag{8a}$$

$$u_z = \tfrac{1}{2}\{zQ_1 + 2U_1\}\cos\phi, \quad p = \mu Q_1\cos\phi, \tag{8b}$$

where Q_1, U_0, U_1 and U_2 are functions of ρ and z satisfying the differential equations

$$L_0^2[U_0] = L_1^2[U_1] = L_1^2[Q_1] = L_2^2[U_2] = 0, \tag{9}$$

in term of the operators

$$L_m^2 = \frac{\partial^2}{\partial\rho} + \frac{1}{\rho}\frac{\partial}{\partial\rho} + \frac{\partial^2}{\partial z^2} - \frac{m^2}{\rho^2}. \tag{10}$$

When expressed in the bipolar coordinates (ξ, η), the functions Q_1, U_0, U_1, U_2 are found to be of the following form:

$$U_1 = c^M(\cosh\xi - \lambda)^{1/2}\sin\eta\sum_{n\geqslant 1} A_n \sinh(\gamma_n\xi)P_n'(\lambda), \tag{11a}$$

$$Q_1 = c^{M-1}(\cosh\xi - \lambda)^{1/2}\sin\eta\sum_{n\geqslant 1} [B_n\cosh(\gamma_n\xi) + C_n\sinh(\gamma_n\xi)]P_n'(\lambda), \tag{11b}$$

$$U_0 = c^M(\cosh\xi - \lambda)^{1/2}\sum_{n\geqslant 0}^{\infty} [D_n\cosh(\gamma_n\xi) + E_n\sinh(\gamma_n\xi)]P_n(\lambda), \tag{11c}$$

$$U_2 = c^M(\cosh\xi - \lambda)^{1/2}\sin^2\eta\sum_{n\geqslant 2} [F_n\cosh(\gamma_n\xi) + G_n\sinh(\gamma_n\xi)]P_n''(\lambda), \tag{11d}$$

where $\lambda = \cos\eta$, $\gamma_n = n + 1/2$, $P_n(\lambda)$ denotes the Legendre polynomial of order n and the primes designate differentiation with respect to λ. The integer M takes the values $M = 0$ for the translation, $M = 1$ for the rotation and shear flow and $M = 2$ for the quadratic flow. This solution also satisfies the condition that u_z vanishes on the $z = 0$ plane wall. Enforcing the additional velocity boundary conditions $u_\rho = u_\phi = 0$ on the wall and the appropriate condition on the sphere surface $(\xi = \alpha)$ provides (**7**) the following relationships:

$$B_n = (n-1)A_{n-1} - (2n+1)A_n + (n+2)A_{n+1} \quad \text{for } n \geqslant 1, \tag{12a}$$

$$C_n = -2k_n\left[\frac{(n-1)}{2n-1}A_{n-1} - A_n + \frac{n+2}{2n+3}A_{n+1}\right] \quad \text{for } n \geqslant 1, \tag{12b}$$

$$D_n = -\tfrac{1}{2}(n-1)nA_{n-1} + \tfrac{1}{2}(n+1)(n+2)A_{n+1} \quad \text{for } n \geqslant 0, \tag{12c}$$

$$E_n = k_n\left[\frac{(n-1)n}{2n-1}A_{n-1} - \frac{(n+1)(n+2)}{2n+3}A_{n+1}\right] - \varphi_n \quad \text{for } n \geqslant 0, \tag{12d}$$

$$F_n = \tfrac{1}{2}\left[A_{n-1} - A_{n+1}\right] \quad \text{for } n \geqslant 2, \tag{12e}$$

$$G_n = -k_n\left[\frac{A_{n-1}}{2n-1} - \frac{A_{n+1}}{2n+3}\right] \quad \text{for } n \geqslant 2, \tag{12f}$$

with the following definitions:

$$k_n = \gamma_n\coth(\gamma_n\alpha) - \coth\alpha \quad \text{for } n \geqslant 0, \tag{13a}$$

$$\varphi_n = 2\sqrt{2}\{\coth(\gamma_n\alpha) - 1\} \quad \text{(translation)}, \tag{13b}$$

$$\varphi_n = 4\sqrt{2}\gamma_n\{\coth(\gamma_n\alpha) - 1\} \quad \text{(shear flow)}, \tag{13c}$$

$$\varphi_n = \frac{4\sqrt{2}}{3}\gamma_n[\coth(\alpha) + 2\gamma_n]\{\coth(\gamma_n\alpha) - 1\} \quad \text{(quadratic flow)}. \tag{13d}$$

Finally, the continuity equation yields in conjunction with the relationships (12) the following infinite linear system for the unknown coefficients $A_n (n \geqslant 1)$:

$$a_{n,n-1}A_{n-1} + a_{n,n}A_n + a_{n,n+1}A_{n+1} = b_n \quad \text{for } n \geqslant 1 \tag{14}$$

with associated coefficients $a_{n,n-1}$, $a_{n,n}$, $a_{n,n+1}$ and b_n defined, for $n \geqslant 1$, as[†]

$$a_{n,n-1} = \frac{n-1}{2n-1}[(2n-1)k_{n-1} - (2n-3)k_n], \tag{15a}$$

$$a_{n,n} = -\frac{1}{2n+1}\{n(2n-1)k_{n-1} + 5(2n+1)k_n - (n+1)(2n+3)k_{n+1}\}, \tag{15b}$$

$$a_{n,n+1} = \frac{n+2}{2n+3}[(2n+5)k_n - (2n+3)k_{n+1}], \tag{15c}$$

$$b_n = \tfrac{1}{2}[\varphi_{n-1} - 2\varphi_n + \varphi_{n+1}]. \tag{15d}$$

Since (**u**, p) vanishes for $|\boldsymbol{r}| \to \infty$, that is, when $(\xi, \eta) \to (0, 0)$, and remains bounded on the wall and in the entire fluid domain, it is clear that A_n and all other coefficients in (12) should vanish as $n \to \infty$. According to (**8**, **9**), the perturbation flow (**u**, p) applies on the fixed sphere a force $F_x \boldsymbol{e}_x$ and a torque $C_y \boldsymbol{e}_y$ (with respect to the centre of the sphere) given by the formulae

$$F_x = c^M \sqrt{2}\pi\,\mu a \sinh\alpha \sum_{n\geqslant 0}\{E_n + n(n+1)C_n\}, \tag{16a}$$

$$C_y = 2c^M \sqrt{2}\pi\,\mu a^2 \sinh^2\alpha \sum_{n\geqslant 0}\{2n(n+1)A_n + E_n \coth\alpha\}. \tag{16b}$$

The resulting friction factors f^{t}_{xx}, c^{t}_{yx}, f^{r}_{xy}, c^{r}_{yy}, f^{s}_{xx}, c^{s}_{yx}, f^{q}_{xx} and c^{q}_{yx}, previously defined in (3) are displayed in Appendix A.1.

3.2 *Sphere held fixed in a modulated straining motion*

As already noticed in (**10**), the perturbation flow (**u**, p) that fulfills the no-slip boundary condition $\mathbf{u} = -z(y\,\mathbf{e}_x + x\,\mathbf{e}_y)$ on $\mathcal{S}$ applies, for symmetry reasons, zero torque and force on the fixed sphere. However, these authors did not determine (**u**, p) in the fluid domain. This is achieved in the present subsection by using the more general solution proposed by (**15**) to obtain the prescribed boundary conditions:

$$u_\rho = -\rho z \sin 2\phi, \quad u_\phi = \rho z \cos 2\phi, \quad u_z = 0 \ \text{ on } \xi = \alpha. \tag{17}$$

The solution, which has not been obtained so far to the authors' very best knowledge, is established by mimicking the treatment of (**7**). Inspecting (17) first suggests to seek the velocity and pressure disturbances $\mathbf{u} = u_\rho \mathbf{e}_\rho + u_\phi \mathbf{e}_\phi + u_z \mathbf{e}_z$ and p in the following forms:

$$u_\rho = U_\rho \sin 2\phi, \quad u_\phi = U_\phi \cos 2\phi, \quad u_z = U_z \sin 2\phi, \quad p = \mu P \sin 2\phi, \tag{18}$$

where U_ρ, U_ϕ, U_z and P only depend upon ρ and z. As detailed in Appendix A.2, if the above flow (**u**, p) satisfies the Stokes equations, the solution may be obtained in the form

$$u_\rho = \tfrac{1}{2}\{\rho Q_2 + W_1 + W_3\} \sin 2\phi, \quad u_\phi = \tfrac{1}{2}(W_1 - W_3) \cos 2\phi, \tag{19a}$$

$$u_z = \tfrac{1}{2}\{z Q_2 + 2W_2\} \sin 2\phi, \quad p = \mu Q_2 \sin 2\phi, \tag{19b}$$

[†]The misprint error for b_n in (**10**, equation (4.24)) is corrected here.

where Q_2, W_1, W_2 and W_3 are functions of ρ and z satisfying the differential equations (recall (10))

$$L_1^2[W_1] = L_2^2[W_2] = L_2^2[Q_2] = L_3^2[W_3] = 0. \tag{20}$$

When expressed in the bipolar coordinates (ξ, η) the solution is obtained from (**6**), using the condition that u_z vanishes on the wall $\xi = 0$ and the pressure is bounded there:

$$W_2 = c^2(\cosh\xi - \lambda)^{1/2}\sin^2\eta \sum_{n\geqslant 2} A_n \sinh(\gamma_n\xi) P_n''(\lambda), \tag{21a}$$

$$Q_2 = c\,(\cosh\xi - \lambda)^{1/2}\sin^2\eta \sum_{n\geqslant 2} [B_n\cosh(\gamma_n\xi) + C_n\sinh(\gamma_n\xi)] P_n''(\lambda), \tag{21b}$$

$$W_1 = c^2(\cosh\xi - \lambda)^{1/2}\sin\eta \sum_{n\geqslant 1} [D_n\cosh(\gamma_n\xi) + E_n\sinh(\gamma_n\xi)] P_n'(\lambda), \tag{21c}$$

$$W_3 = c^2(\cosh\xi - \lambda)^{1/2}\sin^3\eta \sum_{n\geqslant 3} [F_n\cosh(\gamma_n\xi) + G_n\sinh(\gamma_n\xi)] P_n'''(\lambda). \tag{21d}$$

Recall that $\lambda = \cos\eta$ and $\gamma_n = n + 1/2$. These expressions valid for an ambient modulated straining motion are the counterparts of the expressions (11) for the other ambient flow fields. The unknown coefficients in (21), A_n, B_n, C_n for $n \geqslant 2$, D_n, E_n for $n \geqslant 1$ and F_n, G_n for $n \geqslant 3$ are obtained by enforcing not only the remaining boundary conditions at the wall (that is, $u_\rho = u_\phi = 0$ for $\xi = 0$) and on the sphere (see (17)) but also the continuity equation and the far-field behaviour $(\mathbf{u}, p) \to (\mathbf{0}, 0)$ as $(\xi, \eta) \to (0, 0)$. This straightforward but somewhat tedious procedure is detailed in Appendix A.2. The coefficients B_n, C_n, D_n, E_n, F_n and G_n may then be expressed in terms of the coefficients A_n $(n \geqslant 2)$ as follows:

$$B_n = (n-2)A_{n-1} - (2n+1)A_n + (n+3)A_{n+1} \quad (n \geqslant 2), \tag{22a}$$

$$C_n = -2k_n\left\{\frac{(n-2)}{2n-1}A_{n-1} - A_n + \frac{n+3}{2n+3}A_{n+1}\right\} \quad (n \geqslant 2), \tag{22b}$$

$$D_n = -\tfrac{1}{2}(n-2)(n-1)A_{n-1} + \tfrac{1}{2}(n+2)(n+3)A_{n+1} \quad (n \geqslant 1), \tag{22c}$$

$$E_n = k_n\left\{\frac{(n-2)(n-1)}{2n-1}A_{n-1} - \frac{(n+2)(n+3)}{2n+3}A_{n+1}\right\} - r_n \quad (n \geqslant 1), \tag{22d}$$

$$F_n = \tfrac{1}{2}[A_{n-1} - A_{n+1}] \quad (n \geqslant 3), \tag{22e}$$

$$G_n = -k_n\left[\frac{A_{n-1}}{2n-1} - \frac{A_{n+1}}{2n+3}\right] \quad (n \geqslant 3), \tag{22f}$$

with k_n (recall (13a)) and r_n defined as

$$k_n = \gamma_n\coth(\gamma_n\alpha) - \coth\alpha, \quad r_n = -\frac{8\sqrt{2}\gamma_n}{3}\{\coth(\gamma_n\alpha) - 1\} \quad \text{if } n \geqslant 1. \tag{23}$$

Finally, for the reasons invoked in subsection 3.1, $A_n \to 0$ as $n \to \infty$ and obeys the system of linear equations

$$a_{n,n-1}A_{n-1} + a_{n,n}A_n + a_{n,n+1}A_{n+1} = b_n \quad \text{for } n \geqslant 2 \tag{24}$$

with coefficients $a_{n,n-1}$, $a_{n,n}$, $a_{n,n+1}$ and b_n defined, for $n \geqslant 2$, as

$$a_{n,n-1} = \frac{n-2}{2n-1}[(2n-1)k_{n-1} - (2n-3)k_n], \tag{25a}$$

$$a_{n,n} = -\frac{1}{2n+1}\{n(2n-1)k_{n-1} + 5(2n+1)k_n - (n+1)(2n+3)k_{n+1}\}, \tag{25b}$$

$$a_{n,n+1} = \frac{n+3}{2n+3}[(2n+5)k_n - (2n+3)k_{n+1}], \tag{25c}$$

$$b_n = \tfrac{1}{2}[r_{n-1} - 2r_n + r_{n+1}]. \tag{25d}$$

3.3 *Sphere held fixed in a rotational flow or modulated rotational flow*

In this subsection, the ambient external flow is either a rotational flow ($\boldsymbol{u}_\infty = y\,\boldsymbol{e}_x - x\,\boldsymbol{e}_y$) or a modulated rotational flow ($\boldsymbol{u}_\infty = zy\,\boldsymbol{e}_x - zx\,\boldsymbol{e}_y$). Both cases may be considered at the same time by applying the no-slip condition $\boldsymbol{u} = z^l\rho\mathbf{e}_\phi$ with $l = 0, 1$ for the perturbed flow on the sphere. This suggests we write the perturbation velocity as $\mathbf{u} = u_\phi\mathbf{e}_\phi$ in the entire fluid domain, this form satisfying automatically the continuity equation. The momentum equation in cylindrical polar coordinates (ρ, z, ϕ) gives

$$L_1^2[u_\phi] = 0, \quad p = 0. \tag{26}$$

Following (**6**), the solution u_ϕ that vanishes on the $\xi = 0$ plane is written in the form

$$u_\phi = c^{l+1}(\cosh\xi - \cos\eta)^{1/2}\sin\eta\sum_{n\geqslant 1} H_n^{(l)}\sinh(\gamma_n\xi)P_n'(\cos\eta) \quad \text{for } l = 0, 1 \tag{27}$$

with, again, $\gamma_n = n + 1/2$. For symmetry reasons, the axisymmetric flow ($\mathbf{u}$, p) applies a zero force and a couple $C_l\mathbf{e}_z$ on the sphere with (**16**)

$$C_l = -2\pi\mu\int_0^\pi \rho^3\left[\frac{\partial}{\partial\xi}\left(\frac{u_\phi}{\rho}\right)\right]_{\xi=\alpha} d\eta. \tag{28}$$

Using the solution (27) one thus derives, after elementary algebra, the simple formula

$$C_l = -4\sqrt{2}\pi\mu c^{l+3}\sum_{n\geqslant 1} n(n+1)H_n^{(l)}. \tag{29}$$

The required coefficients $H_n^{(l)}$ are obtained by enforcing the velocity boundary condition on the sphere, that is, the relation $H_l(\alpha, \eta) = z^l\rho$. Exploiting the identity

$$(\cosh\alpha - \cos\eta)^{1/2} = 2\sqrt{2}\sum_{n\geqslant 1}\mathrm{e}^{-\gamma_n\alpha}P_n'(\cos\eta)$$

and (A.8), it follows that

$$H_n^{(0)} = \frac{2\sqrt{2}\mathrm{e}^{-\gamma_n\alpha}}{\sinh(\gamma_n\alpha)} \quad \text{and} \quad H_n^{(1)} = \frac{4\sqrt{2}\gamma_n\mathrm{e}^{-\gamma_n\alpha}}{3\sinh(\gamma_n\alpha)} \quad \text{for } n \geqslant 1. \tag{30}$$

These results agree with (**16**) for $l = 0$ and (**10**) for $l = 1$.[‡] Recalling the definitions (3e) of c^{r}_{zz} and (3f) of c^{m}_{zx}, using (29) and the relations $c = a \sinh\alpha$ and $\ell = a\cosh\alpha$, we finally obtain (since the flow field considered in section 3.2 applies zero torque on $\mathcal{S}$)

$$c^{\mathrm{r}}_{zz} = \frac{\sqrt{2}}{2}\sinh^3\alpha \sum_{n\geqslant 1} n(n+1)H^{(0)}_n, \tag{31a}$$

$$c^{\mathrm{m}}_{zx} = \frac{\sqrt{2}\sinh^4\alpha}{2\cosh\alpha} \sum_{n\geqslant 1} n(n+1)H^{(1)}_n. \tag{31b}$$

3.4 *Explicit iterative procedure*

For the axisymmetric flow of section 3.3 the solution is obtained in closed form (see (27), (30), (31a)). By contrast, for the asymmetric flow fields of section 3.1 and section 3.2 it is necessary to solve the infinite linear systems (14), (24) respectively, with $A_n \to 0$ as $n \to \infty$. Note that setting $A'_n = A_{n+1}$ in (24) also yields (14). In the infinite system (14) the first coefficient A_1 is unknown. It is obtained by enforcing the condition $A_n \to 0$ as $n \to \infty$.

In order to obtain accurate values for the perturbation flow ($\mathbf{u}$, p) and the associated force and torque on the sphere, the system (14) should be solved with a high precision for any position of the sphere relative to the plane (even for $\ell/a - 1 \ll 1$). A classical way consists in truncating (14) with $A_{N+1} = 0$ for some large N, solving the resulting linear system for the A_n and repeating the procedure for successively larger values of N until a prescribed accuracy is achieved. Unfortunately, if the gap between the sphere and the wall becomes small the number of terms in the series increases and this results in huge linear systems requiring a large computer memory. Alternative methods, however, exist. For example, the one proposed in (**17**) uses the Thomas algorithm. In the present work we rather follow an iterative procedure pioneered in (**11**) and applied in (**4**, **5**) to determine the coefficients with a high accuracy and a limited computer memory. Further details can be found in (**4**). The drawback is that it is explicit and all intermediate calculations have to be performed with a high precision. Proceeding as in (**4**), we therefore used MAPLE software (which allows to calculate floating point numbers with any precision) and increased in a loop the retained number of digits so as to obtain the required accuracy. In principle, any precision can be obtained; we decided to give here all results with a precision of 5×10^{-17}, which required typically 35 digits in the intermediate calculations. We could then obtain results for small gaps down to 2×10^{-6} by calculating a large number N of coefficients (typically more than 10000).

4. Results and discussion

Consider the undisturbed flow (1). The case of the linear shear flow $\mathbf{u}_\infty = k_{\mathrm{s}} z\,\mathbf{e}_x$ was explored in detail in (**4**). Here, we investigate the remaining term in (1), that is, the quadratic shear flow $k_{\mathrm{q}} z^2\,\mathbf{e}_x$ (section 4.1) and the modulated shear flow $2k_{\mathrm{m}} zy\,\boldsymbol{e}_x$ (section 4.2).

[‡]Note that a misprint occurred in the result (**10**, (3.17)), where ξ should be replaced by α.

Table 1 Dimensionless force f^{q}_{xx} and torque c^{q}_{yx} (also called the friction factors, as defined in $(3d)_{1,2}$, respectively) exerted by a quadratic flow on a fixed sphere centred at a distance ℓ from the wall. GO represent the numbers obtained by (**10**) in tangent-sphere coordinates (for $\ell/a = 1$) and in bipolar coordinates (for $\ell/a > 1$). The other columns contain our results. The displayed digits have been calculated using N harmonics for accuracy. Our value for $\ell/a = 1$ is obtained by extrapolation

ℓ/a	GO			This work	
	f^{q}_{xx}	c^{q}_{yx}	N	f^{q}_{xx}	c^{q}_{yx}
1·0	1·943	0·9907	-	1·9428093729	0·9907705186
1·000002			18639	1·9428069911698754	0·9907704897178268
1·000005			11885	1·942803418541594	0·9907704463397817
1·00001			8456	1·9427974642166769	0·9907703740455426
1·0001			2732	1·9426902982410483	0·9907690732840887
1·001	1·942	0·9907	888	1·9416198743752426	0·9907561213028173
1·005	1·937	0·9907	406	1·9368894693971682	0·9906997696228465
1·01	1·931	0·991	290	1·9310378453544558	0·9906320649887506
1·05	1·887	0·990	136	1·8865513073014267	0·9901908673502305
1·1	1·836	0·990	95	1·8361966587990916	0·989852570880746
1·18			72	1·7658220852369336	0·9896779911554802
1·2			68	1·7499153741475205	0·9896879534804441
1·5	1·568	0.991	44	1·5686405440293652	0·9910961255337066
2·0	1·400	0·999	33	1·399981711095499	0·9942362161231037
4·0			22	1·1752254609536348	0·9988439436952222
5·0	1·135		20	1·1353827710379781	0·9993663652434029
10·0	1·062	1·000	16	1·0623566493117817	0·9999118967578662
21·0	1·028	1·000	13	1·0282170782321677	0·9999901131253082
51·0	1·0113	1·000	11	1·0112763018589653	0·9999992991318837

4.1 *Case of the quadratic shear flow*

In this subsection we provide results for a fixed sphere embedded in the quadratic shear flow $k_{\mathrm{q}} z^2\, \mathbf{e}_x$. Values of the friction factors f^{q}_{xx} and c^{q}_{yx} are listed in Table 1 and compared with the earlier results of (**10**)[§] which have a lower precision of 10^{-3}.

Using the analytical results from the BC method, the friction factors f^{q}_{xx} and c^{q}_{yx} are computed with a precision of 5×10^{-17} in the range $\ell/a \geqslant 1 + 2 \times 10^{-6}$, as explained in section 3.4. The indicated number N of retained harmonics, as defined in section 3.4, is seen to increase significantly as ℓ/a collapses to unity. When the sphere is attached to the wall, that is, for $\ell/a = 1$, the BC method cannot be applied and our results indicated for f^{q}_{xx} and c^{q}_{yx} were obtained by extrapolation.

The force friction coefficient f^{q}_{xx} given in Table 1 is found to monotonically decrease as ℓ/a increases from unity whereas variations of the torque friction coefficient c^{q}_{yx} are quite small. The

[§]Due to a different scaling, the coefficients f_2 and g_2 displayed in (**10**, Table 2) read $f^{\mathrm{q}}_{xx}/\cosh^2\alpha$ and $c^{\mathrm{q}}_{yx}/\cosh\alpha$, respectively.

accuracy of our results allows us to discover a minimum of c_{yx}^{q} at the critical distance $\ell/a \sim 1{\cdot}18$. This subtle behaviour of the coefficient c_{yx}^{q} is exhibited in Fig. 1. By contrast, the results of (**10**) were not accurate enough to detect the existence of such a minimum.

The fluid velocity and pressure are determined from the BC method with a 10^{-6} precision, which is sufficient to describe the flow field. The flow pattern at the critical location $\ell/a = 1{\cdot}18$ is depicted in Fig. 2(a) where the analytical streamlines of the perturbed velocity $z^2\mathbf{e}_x + \mathbf{u}$ are plotted in the $y = 0$ plane (these are streamlines because $(\boldsymbol{u}_\infty + \boldsymbol{u}) \cdot \boldsymbol{e}_y = 0$ in this entire plane, as evidenced by (8a) for $\phi = 0$ or $\phi = \pi$). The isobars are also represented in Fig. 2(b). Typical values of the perturbed velocity and pressure are given in Table 2 for the four points M_k ($k = 1, \ldots, 4$) in the fluid domain represented in Fig. 2(a).

As observed in Fig. 2(a), there are two large vortices of opposite directions right upstream and dowstream of the stationary sphere. However, the centres of the two vortices are not stagnation points since, as illustrated in the three-dimensional view of Fig. 3, they are three-dimensional fluid trajectories around the sphere from the upstream vortex centre to the downstream one. The strong pressure gradient above the sphere (see Fig. 2(b)) is clearly connected to the fact observed in Fig. 3 that the fluid cannot flow below the sphere and thus is pushed above and around it.

As seen in Fig. 2(a), the fluid flows in the $\mathbf{e}_x$ direction near M_2 and in the opposite direction near M_1. This remark is emphasized in Fig. 4(a) which plots the iso-values of the x velocity component in the $x = 0$ plane. This figure shows that, as opposed to the case of an ambient linear shear flow (**4**), there is a large pocket of negative Cartesian disturbed velocity component $(z^2\mathbf{e}_x + \mathbf{u}) \cdot \mathbf{e}_x$ below the sphere. The flow in the vicinity of the points M_1 and M_2 therefore has a positive contribution to the torque coefficient c_{yx}^{q}. By contrast, the flow near the point M_3 and its symmetric with respect to the (O, y, z) plane, that is, the flow related to the two close vortices, induces a negative contribution to c_{yx}^{q}. The behaviour of c_{yx}^{q} displayed in Fig. 1(b) thus results, at least for $\ell/a \sim 1{\cdot}18$, from a competition between the strength of the two detected vortices and the flow structure right above and below the sphere. When the sphere–wall gap increases from zero to $0{\cdot}18\,a$, the flow rate in the $-\boldsymbol{e}_x$ direction increases below the sphere and the vortices become stronger. Above the critical ratio $\ell/a = 1{\cdot}18$, the vortices lie too far from the sphere surface to induce a strong enough negative

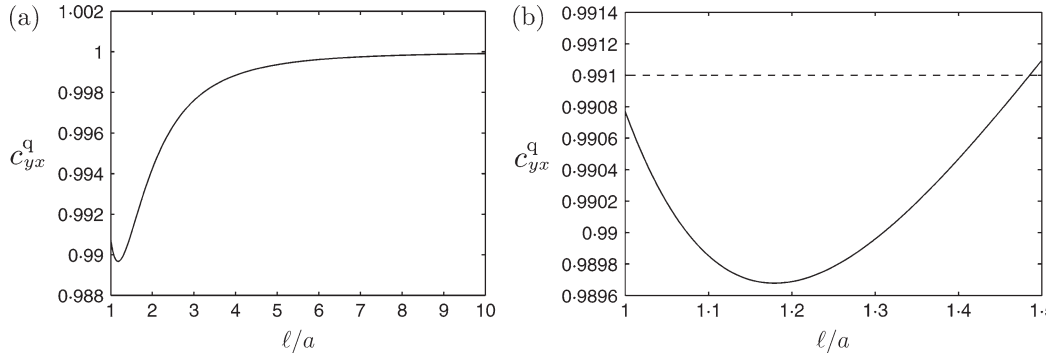

Fig. 1 (a) Non-dimensional coefficient c_{yx}^{q} for the quadratic flow. (b) Magnified plot for a sphere close to the wall. The dashed line indicates the results of (**10**).The smallest value of c_{yx}^{q}, here obtained for $\ell/a \sim 1{\cdot}18$, is found to be $c_{yx}^{\mathrm{q}} = 0{\cdot}989678$.

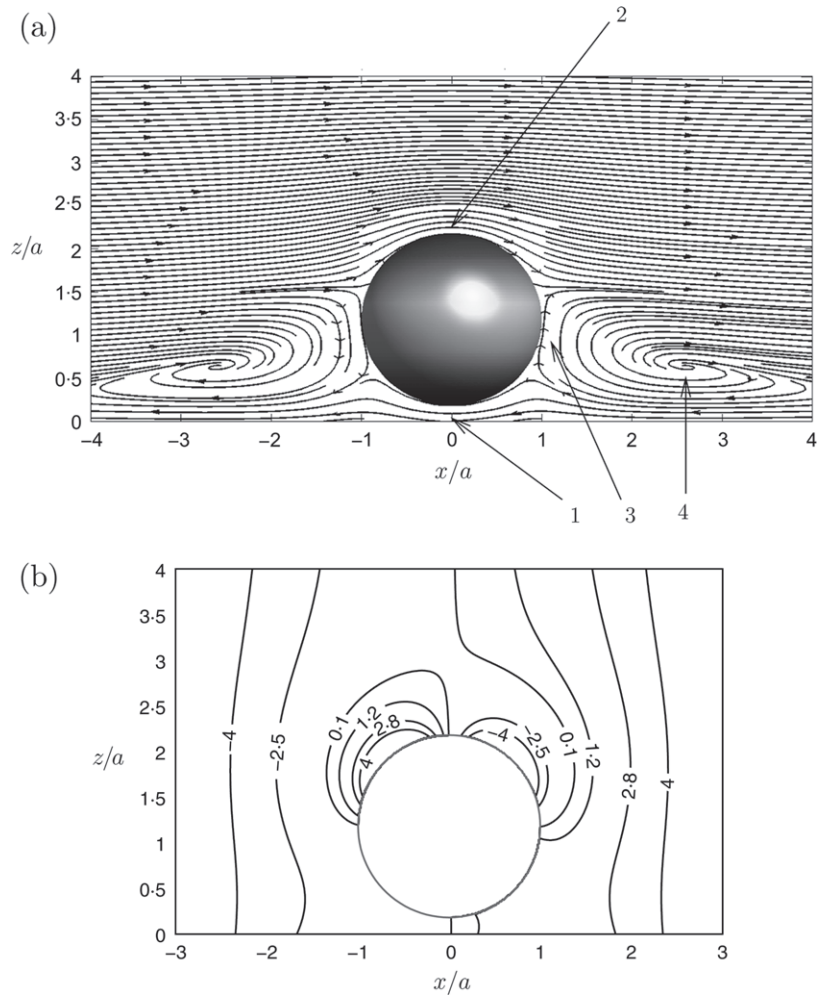

Fig. 2 (a) Perturbed flow $z^2\mathbf{e}_x + \mathbf{u}$ streamlines in the $y = 0$ plane about a sphere held fixed in the quadratic flow $z^2\mathbf{e}_x$ and experiencing the minimum torque at the critical location $\ell = 1{\cdot}18a$. Numbers k indicate the points M_k where the comparisons, reported in Table 2, have been achieved with the bipolar coordinates and the boundary element methods, both for the disturbed velocity $\mathbf{u}_\infty + \mathbf{u}$ and pressure $p_\infty + p$. The Cartesian coordinates of each point M_k are introduced in the legend of Table 2. (b) Isobars of the disturbed quadratic flow in the plane $y = 0$ for $\ell/a = 1{\cdot}18$

contribution to c^{q}_{yx}. Then, as ℓ/a increases, the pocket of negative velocity component $(z^2\mathbf{e}_x + \mathbf{u}).\mathbf{e}_x$ shrinks, as depicted in Fig. 4(b) for $\ell/a = 5$, and eventually disappears for $\ell/a \sim 20$. Note that for $\ell/a = 5$ the fluid in the vicinity of the z-axis and below the sphere (that is, between the sphere and wall) flows downstream (that is, in the $x > 0$ direction) except near the wall. It is also found that the two depicted opposite vortices remain close to the wall and therefore far from the sphere

Table 2 Dimensionless perturbed fluid velocity and pressure close to a sphere fixed in an ambient quadratic flow. The sphere centre is at $\ell/a = 1.18$. The normalized perturbed velocity components V_x, V_z and pressure P defined by (34) are evaluated at the four points M_k ($k = 1, 2, 3, 4$) indicated in Fig. 2. The Cartesian coordinates of the point M_k are $(x_k, 0, z_k)$, with $x_1 = x_2 = 0$, $x_3/a = 1{\cdot}18$, $x_4/a = 2{\cdot}5$, $z_1/a = 0{\cdot}09$, $z_2/a = 2{\cdot}27$, $z_3/a = 1$ and $z_4/a = 0{\cdot}55$. Note that, for symmetry reasons, $V_y = 0$ in the entire $y = 0$ plane

Perturbed fluid velocity and pressure	Point M_1	Point M_2	Point M_3	Point M_4
V_x	−0·018624	1·392969	0·012304	−0·084980
V_z	0	0	0·145723	0·005616
P	0	0	1·342334	4·391804

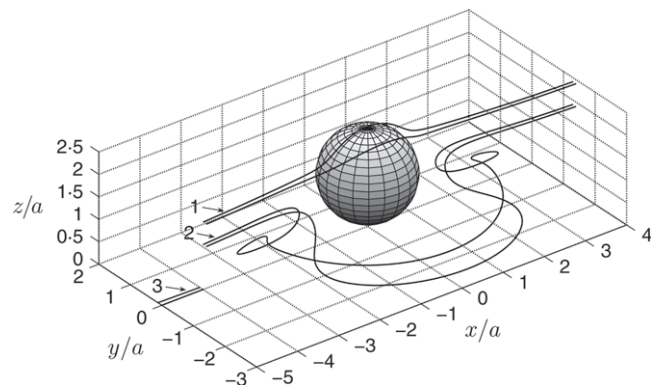

Fig. 3 Perturbed flow $z^2\mathbf{e}_x + \mathbf{u}$ around a sphere centred at the critical distance $\ell = 1{\cdot}18a$ from the wall. Six three-dimensional trajectories starting from points at $x = -4a$ and either very close (curves labelled 1, 2, 3 with $y = -10^{-4}a$) or close (with $y = -10^{-1}a$) to the $y = 0$ plane. The initial z-value for trajectories labelled 1, 2, 3 (and neighbouring ones) are $1{\cdot}5a$, a, $0{\cdot}002a$, respectively

as ℓ/a increases. For instance, the streamlines associated to the perturbed velocity $z^2\mathbf{e}_x + \mathbf{u}$ for $\ell/a = 10$ plotted in Fig. 5(a) clearly illustrate this feature. The three-dimensional flow field structure (not shown here) is similar to the one depicted in Fig. 3. As announced, the fluid flows in the $\boldsymbol{e}_x$ direction both above and below the sphere in the $x = 0$ plane for $\ell/a = 10$.

At this stage one may wonder whether the observed near-wall vortices are due to the no-slip condition at the plane wall. This issue is addressed by determining the perturbed flow about a sphere held fixed in the *unbounded* quadratic flow $z^2\mathbf{e}_x$, that is, in the absence of the wall. Using the singularity method as in (**18**) one obtains, as shown in Appendix A.3, the required velocity $z^2\mathbf{e}_x + \mathbf{u}$. The resulting (disturbed) streamlines pattern is displayed in the $y = 0$ plane and for the ratio $\ell/a = 10$ in Fig. 5(b) for comparison with Fig. 5(a). The streamlines around $z = 4$ are not

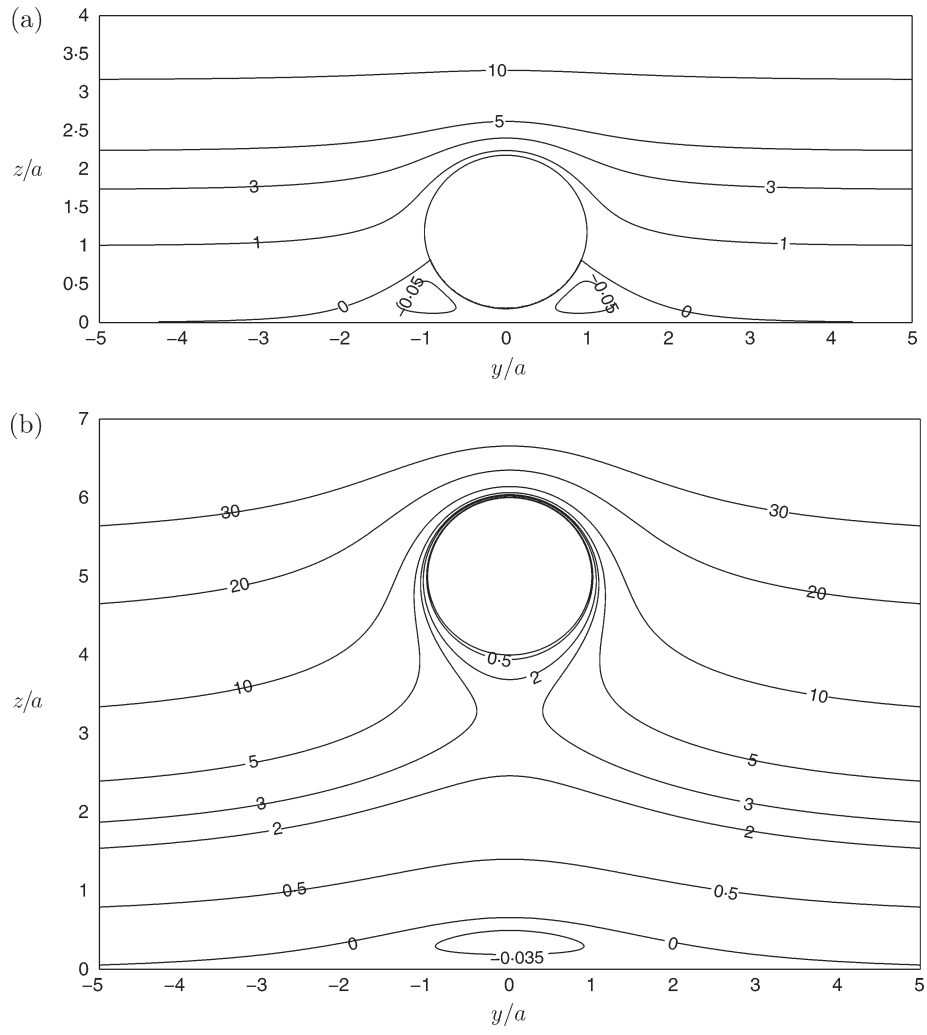

Fig. 4 Lines of iso-values of the Cartesian disturbed velocity component $(\boldsymbol{u}_\infty + \boldsymbol{u}) \cdot \boldsymbol{e}_x$ in the $x = 0$ plane for a sphere held fixed in the quadratic flow $z^2\boldsymbol{e}_x$. (a) Case of the critical ratio $\ell/a = 1{\cdot}18$. (b) Case $\ell/a = 5$

vortices but open trajectories which match the quadratic flow at infinity. There is only one vortex located in the $z < 0$ domain. The pair of vortices in Fig. 5(a) is thus due to the wall.

The high accuracy allowed by the BC method makes it possible to build interpolation formulae both for the force and the torque friction factors f^{q}_{xx} and c^{q}_{yx}, using the calculated values in the range $\ell/a \geqslant 1 + 2 \times 10^{-6}$. For a sphere held fixed close to a motionless wall in an external viscous flow, there is no relative motion of surfaces and therefore for a vanishing gap $\ell/a - 1$ no lubrication singularity. Hence, there is no singular logarithmic term in $\ell/a - 1$ for the force and torque experienced by the sphere unlike the cases of translation and rotation (parallel to the wall)

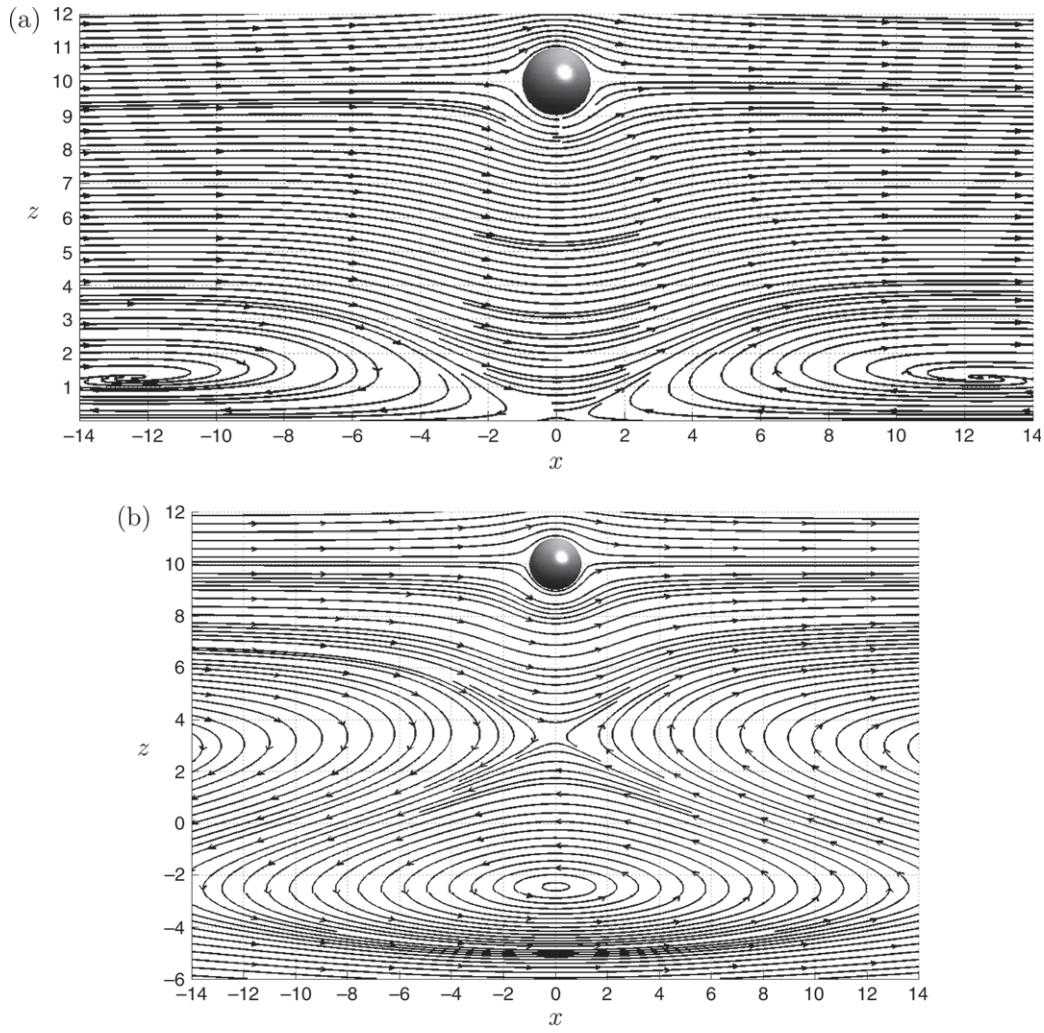

Fig. 5 Perturbed flow $z^2\mathbf{e}_x + \mathbf{u}$ streamlines in the $y = 0$ plane about a sphere held fixed in the parabolic shear flow $z^2\mathbf{e}_x$ for $\ell/a = 10$. (a) Sphere in the presence of the rigid stationary $z = 0$ plane wall. (b) Sphere immersed in an unbounded fluid (that is, without the no-slip velocity boundary condition at $z = 0$)

treated in (**19**). In searching interpolation formulae using the method of least squares we did not find regular logarithmic expansions. The following polynomial interpolations:

$$f^{\mathrm{q}}_{xx} = \sum_{n=0}^{16} g^{\mathrm{q}}_n \left(1 - \frac{a}{\ell}\right)^n, \quad c^{\mathrm{q}}_{xx} = \sum_{n=0}^{16} d^{\mathrm{q}}_n \left(1 - \frac{a}{\ell}\right)^n \quad \text{for } \ell/a \geqslant 1 + 2 \times 10^{-6}, \tag{32}$$

with coefficients g^{q}_n and d^{q}_n given in Table 6 provide a 10^{-9} accuracy. A comparable precision is expected also for smaller values, down to $\ell/a = 1$, because both friction factors are smooth, slowly

varying bounded functions in this limit. Note that the variable $1 - a/\ell$ was found to be appropriate since all coefficients in Table 6 are of order unity.

The translational and rotational velocities of a freely suspended sphere in the ambient quadratic flow $k_{\mathrm{q}} z^2 \boldsymbol{e}_x$ are then calculated from the friction coefficients using formulae (5b). The normalized translational (6a) and rotational (6b) velocities are represented in Fig. 6. Clearly, as compared with a freely moving sphere in unbounded fluid, the sphere translational and rotational motions are slower because of hydrodynamic interactions with the wall when the centre to wall distance is smaller than about three times its radius. Both velocities decrease rapidly when the gap becomes small and eventually vanish at contact. Results for U^{q} and Ω_y^{q} are presented in Table 3. Note that $\Omega_y^{\mathrm{q}} > U^{\mathrm{q}}$ because of the normalization of these quantities. But taking the normalized quantities $\tilde{\Omega}_y^{\mathrm{q}}$ and $\tilde{U}^{\mathrm{q}}$ gives more insight into the 'rolling' or 'slipping' like behaviour: the ratio $\tilde{\Omega}_y^{\mathrm{q}}/\tilde{U}^{\mathrm{q}}$ displayed in Fig. 7 is seen to be less than unity. A freely moving sphere in the vicinity of the wall then slides when rotating and translating. The ratio $\tilde{\Omega}_y^{\mathrm{q}}/\tilde{U}^{\mathrm{q}}$ decreases monotonically in most of the range of distances as ℓ/a increases. However, when the sphere is very close to the wall there is a maximum of $\tilde{\Omega}_y^{\mathrm{q}}/\tilde{U}^{\mathrm{q}}$ (as shown in the insert in Fig. 7). As remarked in (**13**), the limit value of the ratio $\tilde{\Omega}_y^{\mathrm{q}}/\tilde{U}^{\mathrm{q}}$ at contact is

$$\lim_{\ell/a\to 1} \frac{\tilde{\Omega}_y^{\mathrm{q}}}{\tilde{U}^{\mathrm{q}}} = \lim_{\ell/a\to 1} \frac{16 c_{yx}^{\mathrm{q}} + 3 f_{xx}^{\mathrm{q}}}{4(c_{yx}^{\mathrm{q}} + 3 f_{xx}^{\mathrm{q}})}. \tag{33}$$

With the calculated values of f_{xx}^{q} and c_{yx}^{q} at contact ($\ell = a$), given in Table 1, formula (33) gives the limit value 0·7948425310.

4.2 *Case of the modulated shear flow*

In this subsection results are presented for a sphere either held fixed or freely suspended in the external modulated shear flow $2k_{\mathrm{m}} zy\, \boldsymbol{e}_x$. As noticed in section 2, the sphere experiences a zero

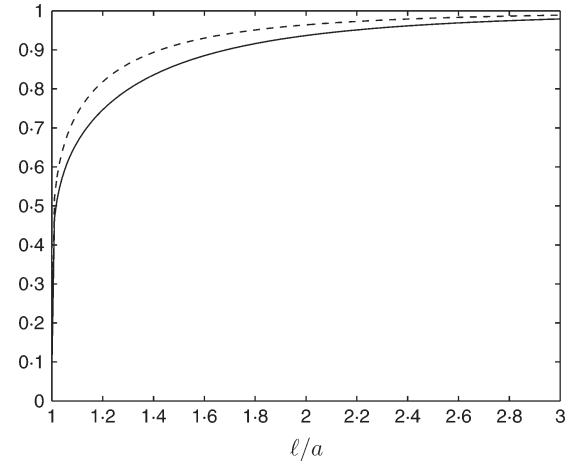

Fig. 6 Normalized translational velocity U^{q}, equation (6a), (solid line) and angular velocity Ω_y^{q}, equation (6b), (dashed line) of a freely suspended sphere in the ambient quadratic flow $k_{\mathrm{q}} z^2 \boldsymbol{e}_x$

Table 3 Dimensionless translational velocity U^{q} and angular velocity Ω_y^{q} (also called mobility coefficients, as defined in (6a), (6b), respectively) of a sphere moving freely in an ambient quadratic flow with its centre at a distance ℓ from the wall

ℓ/a	U^{q}	Ω_y^{q}
1·000002	0·2161061590646320	0·2336866110932329
1·000005	0·2294166837813409	0·2484360152957224
1·00001	0·2406265623723410	0·2608952608866086
1·0001	0·2872281377357567	0·3130726412399164
1·001	0·3560609938079604	0·3912789541877235
1·005	0·4272037859600705	0·4732600366715157
1·01	0·4670018215001825	0·5193133178867895
1·05	0·5915594158991740	0·6607431075765295
1·1	0·6632468634793257	0·7371556465619242
1·18	0·7331924694487259	0·8058528255975131
1·2	0·7464632504325890	0·8181196472757272
1·5	0·8635496899936087	0·9146775770556315
2·0	0·9367346605429616	0·9641487658529515
4·0	0·9908714455773604	0·9952880973012159
5·0	0·9952203858995804	0·9975607934040421
10·0	0·9993825919436270	0·9996897015885476
21·0	0·9999327070366851	0·9999663141041392
51·0	0·9999952907394636	0·9999976449020174

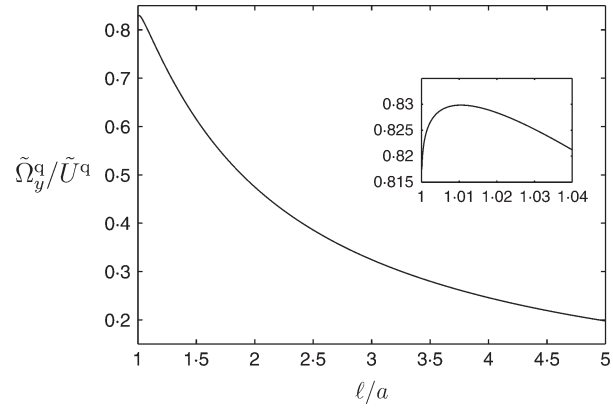

Fig. 7 Ratio $\tilde{\Omega}_y^{\mathrm{q}}/\tilde{U}^{\mathrm{q}}$ for a sphere freely suspended in the ambient quadratic flow $k_{\mathrm{q}} z^2 \boldsymbol{e}_x$. As illustrated by the magnified plot in the range $\ell/a \leqslant 1{\cdot}04$, the ratio $\tilde{\Omega}_y^{\mathrm{q}}/\tilde{U}^{\mathrm{q}}$ exhibits a maximum value $\tilde{\Omega}_y^{\mathrm{q}}/\tilde{U}^{\mathrm{q}} \sim 0{\cdot}83$ at $\ell/a \sim 1{\cdot}01$

Table 4 Dimensionless torque (also called the friction factor c_{zx}^{m}), see (3f), exerted by a modulated shear flow on a sphere centred at a distance ℓ from a wall. GO represent the numbers obtained by Goren and O'Neill (**10**) in tangent-sphere coordinates (for $\ell/a = 1$) and in bipolar coordinates (for $\ell/a > 1$). The other columns contain our result. The displayed digits have been obtained by using N harmonics in the BC method

ℓ/a	GO	Bipolar (this work)	
	c_{zx}^{m}	N	c_{zx}^{m}
1·0	1·082	-	1·08232323371114
1·000002		19243	1·0823228586383199
1·000005		11944	1·0823222960331069
1·00001		8325	1·0823213583684568
1·0001		2505	1·0823044826926661
1·001	1·082	752	1·0821359640887292
1·005	1·081	324	1·0813922016793062
1·01	1·080	225	1·0804743246201650
1·05	1·073	97	1·0735791377038244
1·1	1·066	68	1·0659688546427451
1·2		47	1·0534954376152213
1·5	1·031	30	1·0303567293188152
2·0	1·014	21	1·0139336934667268
4·0		13	1·0018959700828119
5·0	1·001	12	1·0009810108318353
10·0	1·000	9	1·0001243906658378
21·0	1·000	7	1·0000134823415187
51·0	1·000	6	1·0000009421420764

force and the torque given by (3f). The calculated values of c_{zx}^{m} are listed and compared to the predictions of (**10**)[¶] in Table 4 for different values of the normalized sphere to wall distance ℓ/a. The two sets of results are in excellent agreement. The coefficient c_{zx}^{m} is non-singular as $\ell/a - 1$ vanishes and the value of c_{zx}^{m} for $\ell/a = 1$ in the 'bipolar coordinates' column was obtained by extrapolation based on our results for $\ell/a \geqslant 1 + 2 \times 10^{-6}$. Note that for $\ell/a = 1$, the exact value $c_{zx}^{\mathrm{m}} = \pi^4/90$ established in (**10**) is recovered precisely by the BC with a 10^{-14} accuracy. (The multipole expansion which can treat directly the case of contact is applied to this case in (**13**) and provides 32 digits.)

The new solution presented in section 3.2 provides the possibility to compute the perturbed velocity and pressure fields about a sphere held fixed in the ambient modulated straining flow $k_{\mathrm{m}} z(y\mathbf{e}_x + x\mathbf{e}_y)$. The dimensionless velocity and pressure

$$\boldsymbol{V}' = \frac{\boldsymbol{u}_\infty + \boldsymbol{u}}{u^*}, \qquad P' = \frac{a}{\mu u^*}(p_\infty + p) \tag{34}$$

[¶]With our notation the coefficient g_0 displayed in (**10**, Table 1) reads $g_0 = c_{zx}^{\mathrm{m}} \cosh\alpha$.

Table 5 Dimensionless perturbed velocity and pressure close to a sphere fixed in the ambient modulated straining and modulated shear flows, denoted by $(\mathbf{V}', P')$ and $(\mathbf{V}, P)$, respectively (and defined as in (34)). The sphere is located at $\ell/a = 1{\cdot}5$. Results are given at three control points N_1, N_2 and N_3. The Cartesian coordinates of point N_k are (x_k, y_k, z_k) and its distance from the sphere surface is denoted by d_k with $x_k/a = -\sqrt{3}(1{\cdot}1)/2$, $y_k/a = 1{\cdot}1/2$, $z_1/a = 0{\cdot}5$, $z_2/a = 1$, $z_2/a = 1{\cdot}5$, $d_1 = d_3 \sim 0{\cdot}4866a$ and $d_2 = 0{\cdot}1a$. These three control points are represented as dots in Fig. 8

Ambient flow	Perturbed velocity and pressure	Point N_1	Point N_2	Point N_3
$k_m(zy\,\boldsymbol{e}_x + zx\,\boldsymbol{e}_y)$	V_x'	0·073274	−0·096337	0·012304
	V_y'	−0·335637	−0·321480	−1·914931
	V_z'	−0·102882	−0·047419	0·423086
	P'	0·978834	5·111797	1·680545
$2k_m zy\,\boldsymbol{e}_x$	V_x	0·216200	0·113334	1·867243
	V_y	−0·088083	0·041680	−0·090547
	V_z	−0·102882	−0·047419	0·423086
	P	0·978834	5·111797	1·680545

were calculated for $\ell/a = 1{\cdot}5$ at three points in the fluid domain and results are presented in Table 5. This table also also provides the perturbed velocity $\mathbf{V}$ and pressure P (with definitions as in (34)) about the sphere at rest in the modulated shear flow $2k_m yz\mathbf{e}_x$, that is, by adding $(\mathbf{V}', P')$ to the solution obtained in section 3.3 with $l = 1$. As for the quadratic flow, the results from the BC method were calculated with a 10^{-6} precision, sufficient for a description of the flow field.

The flow field associated with the disturbed modulated shear flow $2k_m yz\mathbf{e}_x$ for $\ell/a = 1{\cdot}5$ is illustrated by displaying in Fig. 8 a few three-dimensional fluid trajectories. For symmetry and clarity reasons, attention is confined to the trajectories of twelve fluid particles located at some initial time upstream of the sphere in the $x/a = -6$ plane and in the $y > 0$ domain. As revealed by Fig. 8, some particles flow downstream of the sphere in the $y > 0$ domain (that is, in the positive x direction) whilst other ones turn, cross the $y = 0$ plane before reaching the $x = 0$ plane and move eventually downstream in the $y < 0$ domain (that is, towards the negative x direction). This peculiar behaviour of course did not appear in the previously addressed case of the ambient quadratic flow, since the ambient velocity was then always in the positive x direction. Here, fluid particles close to the $y = 0$ plane are subjected to a low shear rate and they are moreover slowed down by the sphere so that they cannot continue in the positive x direction. Only close enough to the sphere does this effect occur: compare the turning trajectory starting from $x/a = -6, y/a = 0{\cdot}6, z/a = 2{\cdot}2$ with the one starting from $x/a = -6, y/a = 0{\cdot}6, z/a = 3{\cdot}2$ that is extending downstream in the positive x direction. These turning trajectories even occur for a large ℓ/a if the fluid particle originating from the $x/a = -6$ plane moves first towards the gap region between the sphere and the wall, as evidenced by Figs 9(a) and 9(b) which depict 24 fluid trajectories for $\ell/a = 5{\cdot}7$ and $\ell/a = 5{\cdot}8$, respectively. In Fig. 9(a), for $\ell/a = 5{\cdot}7$, all the trajectories issued from the points $x/a = -6$, $y/a = 0{\cdot}1, 0{\cdot}6$, with values of z between the sphere and the wall are turning ones.

Table 6 Coefficients g_n^{q} and d_n^{q} in the polynomial interpolations (32) of the force and torque friction factors f_{xx}^{q} and c_{yx}^{q} on a sphere held fixed in the ambient quadratic flow $z^2\mathbf{e}_x$

n	g_n^{q}	d_n^{q}
0	1·942809372935950	0·990770518637149
1	−1·190886474138724	−0·014458963423686
2	0·197971179572161	0·048012978508492
3	0·017153028426237	0·000110448375706
4	0·008791133201471	−0·000918674215846
5	0·014515813769418	−0·054535006369331
6	−0·008336629006467	0·044760170420802
7	−0·032798221918260	−0·057505664614034
8	0·276562064410017	0·036438908565082
9	−0·666156350582494	0·037436172197695
10	0·832011121112022	−0·018566384980943
11	−0·865119590949199	−0·007424363742828
12	1·732985787425625	−0·038157185515549
13	−2·983624227165502	0·052456242686364
14	2·787095976521595	−0·018167543057367
15	−1·311503308081364	−0·001651453024201
16	0·248529324537360	0·001399799553351

On the other hand for $\ell/a = 5{\cdot}8$, Fig. 9(b), trajectories starting from $x/a = -6$, $y/a = 0{\cdot}6$ are turning ones provided they are close enough to either the sphere or wall, while the ones in the central part of the gap, namely the ones starting from $1{\cdot}9 < z/a < 2{\cdot}6$ are found to extend downstream in the $x > 0$ domain. The trajectory starting from $s = 2{\cdot}2$ illustrates this behaviour. It thus appears that for for $\ell/a = 5{\cdot}7$ there is practically a dead-water region in the gap, that the Stokes flow avoids so as to dissipate the least possible energy. This region can eventually be crossed in its middle for large enough ℓ/a starting from some critical value around $\ell/a = 5{\cdot}8$.

5. Conclusions

In summary, a complete set of results obtained by the BC method is made available for the problems involving a sphere embedded in a second degree polynomial flow along a wall. For the case of an ambient modulated shear flow $2k_{\mathrm{m}}zy\,\boldsymbol{e}_x$, we derived a new solution in BC by extending the treatment of (**7**). We chose to give numerical results for the friction factors in all cases with a 5×10^{-17} accuracy. This was achieved on a personal computer by applying an iteration procedure pioneered by (**11**) and applied with success to the cases of a linear shear flow and a translating and rotating sphere in a fluid at rest by (**4**). We also calculated the force and torque friction coefficients on a sphere fixed in a quadratic or a modulated shear flow with this accuracy even for gaps between the sphere and the wall down to 2×10^{-6} sphere radius. For the quadratic flow, we discovered a minimum value of the torque friction factor c_{yx}^{q} at the critical location $\ell \sim 1{\cdot}18\,a$. This minimum

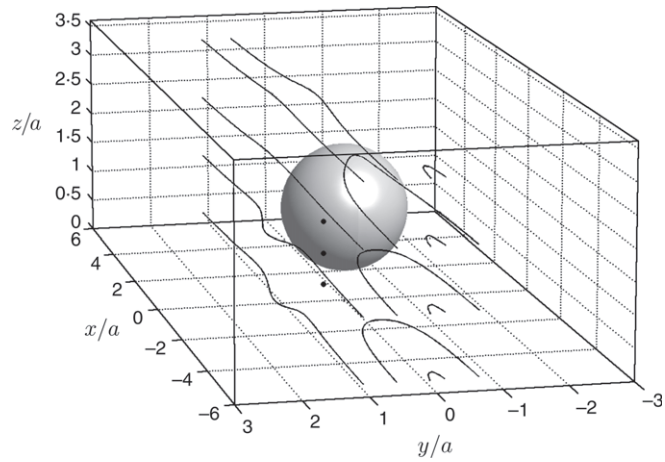

Fig. 8 Twelve three-dimensional fluid trajectories about a sphere held fixed at $\ell/a = 1{\cdot}5$ in the ambient 'modulated' shear flow $2k_{\mathrm{m}}yz\boldsymbol{e}_x$. These trajectories originate from the points with coordinates $x/a = -6$, $y/a = 0{\cdot}1,\ 0{\cdot}6,\ 1{\cdot}1$, $z/a = 0{\cdot}2,\ 1{\cdot}2,\ 2{\cdot}2,\ 3{\cdot}2$. The perturbed fluid velocity and pressure at the three control points represented as dots are given in Table 5

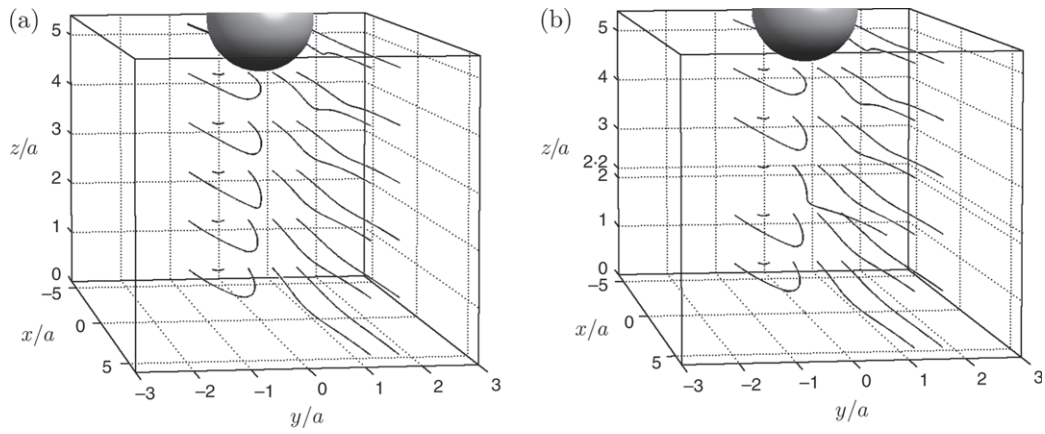

Fig. 9 Counterpart of Fig. 8 but for 24 trajectories originating from the points with coordinates $x/a = -6$, $y/a = 0{\cdot}1,\ 0{\cdot}6,\ 1{\cdot}1,\ 1{\cdot}6$, $z/a = 0{\cdot}2,\ 1{\cdot}2,\ 2{\cdot}2,\ 3{\cdot}2,\ 4{\cdot}2,\ 5{\cdot}2$. (a) Case $\ell/a = 5{\cdot}7$. (b) Case $\ell/a = 5{\cdot}8$

was explained by determining the associated flow structure. The BC method can treat all distances, except the sphere in contact with the wall. Results for this case were calculated by extrapolation with 10^{-11} accuracy from the data for $\ell/a \geqslant 1 + 2 \times 10^{-6}$. By contrast, the multipole expansion can treat all the distances, including contact. The corresponding results are given in the companion article (**13**).

The accuracy of the results also allowed us to provide for the friction factors f^{q}_{xx} and c^{q}_{yx} polynomial interpolation formulae which approximate the exact results in the range $\ell/a \geqslant 1 + 2 \times 10^{-6}$ with a 10^{-9} precision. The normalized translational and rotational velocities, or mobilities, of a freely moving and rotating sphere in a quadratic flow were calculated also with 5×10^{-17} accuracy by combining the present results for the quadratic flow to those of (**4**) for the translating and rotating sphere. Results for the fluid velocity and pressure of the flow fields calculated here were given with a 10^{-6} accuracy, sufficient to determine their features.

All these numerical results provide a base of comparison for other methods which can consider more general geometries. In particular, a detailed study of the accuracy of the multipole expansion in calculating the friction factors and sphere velocities is presented in (**13**).

More general ambient flow fields may be considered by combining the results of this article with the ones calculated with the BC method by (**4**) for the translating, rotating sphere and sphere in shear flow and by (**5**) for the ambient axisymmetrical stagnation point flow $z(x\mathbf{e}_x + y\mathbf{e}_y - z\mathbf{e}_z)$. Note that in the presence of a stagnation point flow the sphere centre translational velocity has a non-zero component normal to the wall. This problem can be treated by combining the preceding results with those for a sphere translating normal to a wall in a fluid at rest (see (**20**, **21**) for the friction factor and (**5**) for the fluid velocity and pressure). Examples of application are the motion of a particle close to a wall in a boundary layer (in a flow along a wall or in a stagnation point flow) and the motion of a particle in a Poiseuille flow. In this latter case, the solution taking one wall into account should be compared with other solutions which consider the two walls. That problem will be treated elsewhere in connection with chemical engineering applications.

The analytical results developed here make it also possible to calculate accurately the stresslet (**22**) exerted on a sphere in a flow field parallel to a plane wall. This quantity plays a key role when evaluating the viscosity of a dilute bounded suspension. This problem is under current investigation.

References

1. M. Martin, Theory of field-flow fractionation, *Advances in Chromatography* (eds P. R. Brown and E. Grushka; Dekker, New York 1998) 1–138.
2. J. Happel and H. Brenner, *Low Reynolds Number Hydrodynamics* (Martinus Nijhoff, The Hague 1973).
3. F. Feuillebois, Some theoretical results for the motion of solid spherical particles in a viscous fluid, *Multiphase Science and Technology*, Vol. 4 (eds G. F. Hewitt, J. M. Delhaye and N. Zuber; Hemisphere, New York 1989) 583–798.
4. M. Chaoui and F. Feuillebois, Creeping flow around a sphere in shear flow close to a wall, *Q. Jl Mech. Appl. Math.* **56** (2003) 381–410.
5. L. Pasol, M. Chaoui, S. Yahiaoui and F. Feuillebois, Analytical solutions for a spherical particle near a wall in axisymmetrical polynomial creeping flows, *Phys. Fluids* **17** (2005) 073602.
6. G. B. Jeffery, On a form of the solution of Laplace's equation suitable for problems relating to two spheres, *Proc. R. Soc.* A **87** (1912) 109–120.
7. W. R. Dean and M. E. O'Neill, A slow rotation of viscous liquid caused by the rotation of a solid sphere, *Mathematika* **10** (1963) 13–24.
8. M. E. O'Neill, A slow motion of viscous liquid caused by a slowly moving solid sphere, *ibid.* **11** (1964) 67–74.
9. M. E. O'Neill, A slow motion of viscous liquid caused by a slowly moving solid sphere: an addendum. *ibid.* **14** (1967) 170–172.

10. S. L. Goren and M. E. O'Neill, On the hydrodynamic resistance to a particle of a dilute suspension when in the neighborhood of a large obstacle, *Chem. Engng Sci.* **26** (1971) 325–338.
11. M. E. O'Neill and B. S. Bhatt, Slow motion of a solid sphere in the presence of a naturally permeable surface, *Q. Jl Mech. Appl. Math.* **44** (1991) 91–104.
12. M. E. O'Neill, A sphere in contact with a plane wall in a slow shear flow, *Chem. Engng Sci.* **11** (1968) 1293–1298.
13. M. L. Ekiel-Jeżewska and E. Wajnryb, Accuracy of the multipole expansion applied to a sphere in a creeping flow parallel to a wall, *Q. Jl Mech. Appl. Math.* **59** (2006) 563–585.
14. L. G. Leal, Particle motions in a viscous fluid, *Ann. Rev. Fluid Mech.* **12** (1980) 435–476.
15. C. J. Lin, K. J. Lee and N. F. Sather, Slow motion of two spheres in a shear field, *J. Fluid Mech.* **43** (1970) 35–47.
16. G. B. Jeffery, On the steady rotation of a solid of revolution in a viscous fluid. *Proc. London Math. Soc.* (2) **14** (1915) 327–338.
17. A. Z. Zinchenko, The slow asymmetric motion of two drops in a viscous medium, *Prikl. Math. Meh.* **44** (1981) 30–37.
18. A. T. Chwang and T. Y. Wu, Hydromechanics of low-Reynolds-number flow. Part 2. Singularity method for Stokes flow, *J. Fluid Mech.* **67** (1975) 787–815.
19. A. J. Goldman, R. G. Cox and H. Brenner, Slow viscous motion of a sphere parallel to a plane wall. I. Motion through a quiescent flow, *Chem. Engng Sci.* **22** (1967a) 637–651.
20. H. Brenner, The slow motion of a sphere through a viscous fluid towards a plane surface, *Chem. Eng. Sci.* **16** (1961) 242–251.
21. A. D. Maude, End effects in a falling-sphere viscometer, *British J. of Appl. Physics* **12** (1961) 293–295.
22. G. K. Batchelor, The stress system in a suspension of force-free particles, *J. Fluid Mech.* **41** (1970) 545–570.

APPENDIX

Details of the BC method

A.1 *Friction factors occurring in Section* 3.1

All friction factors $f^{\mathrm{t}}_{xx}, c^{\mathrm{t}}_{yx}, f^{\mathrm{r}}_{xy}, c^{\mathrm{r}}_{yy}, f^{\mathrm{s}}_{xx}, c^{\mathrm{s}}_{yx}, f^{\mathrm{q}}_{xx}$ and c^{q}_{yx} defined by (3a), (3b), (3c), (3d) are determined by using the formulae (16) and the relationships $c = a\sinh\alpha$ and $\ell = a\cosh\alpha$:

$$f^{\mathrm{t}}_{xx} = \frac{\sqrt{2}S\sinh\alpha}{6}, \quad c^{\mathrm{t}}_{yx} = \frac{\sqrt{2}S'\sinh^2\alpha}{4}, \tag{A.1a}$$

$$f^{\mathrm{r}}_{xy} = -\frac{\sqrt{2}S\sinh^2\alpha}{6}, \quad c^{\mathrm{r}}_{yy} = -\frac{\sqrt{2}S'\sinh^3\alpha}{4}, \tag{A.1b}$$

$$f^{\mathrm{s}}_{xx} = -\frac{\sqrt{2}S\sinh^2\alpha}{6\cosh\alpha}, \quad c^{\mathrm{s}}_{yx} = \frac{\sqrt{2}S'\sinh^3\alpha}{2}, \tag{A.1c}$$

$$f^{\mathrm{q}}_{xy} = -\frac{\sqrt{2}S\sinh^3\alpha}{6}\cosh^2\alpha, \quad c^{\mathrm{q}}_{yx} = \frac{\sqrt{2}S'\sinh^2\alpha}{4}\cosh\alpha, \tag{A.1d}$$

$$S = \sum_{n\geqslant 0}[E_n + n(n+1)C_n], \quad S' = \sum_{n\geqslant 0}[2n(n+1)A_n + E_n\coth\alpha]. \tag{A.1e}$$

A.2 *Calculation of the perturbation flow for the modulated straining motion*

As explained in section 3.2, the perturbation flow $(\mathbf{u}, p)$ for the modulated straining motion is given by equations (18) with unknown functions U_ρ, U_ϕ, U_z and P only depending on (ρ, z). Introducing the vector $\mathbf{a} = \mathbf{u} - p\boldsymbol{x}/(2\mu) = \sin 2\phi[A_\rho \mathbf{e}_\rho + A_z \mathbf{e}_z] + A_\phi \cos 2\phi \mathbf{e}_\phi$ thus yields

$$A_\rho = U_\rho - \frac{\rho}{2}P, \quad A_\phi = U_\phi, \quad A_z = U_z - \frac{z}{2}P, \quad p = \mu P \sin 2\phi. \tag{A.2}$$

From Stokes equations $\boldsymbol{\nabla}^2\mathbf{a} = \mathbf{0}$. Recalling the definition (10) of the operator L^2_m it follows that

$$L^2_2[A_\rho] - \frac{A_\rho}{\rho^2} + \frac{4A_\phi}{\rho^2} = L^2_2[A_\phi] - \frac{A_\phi}{\rho^2} + \frac{4A_\rho}{\rho^2} = 0, \quad L^2_2[A_z] = L^2_2[P] = 0. \tag{A.3}$$

Setting $A_\rho + A_\phi = W_1$, $A_\rho - A_\phi = W_3$, $A_z = W_2$ and $P = Q_2$ gives equations (20) and the relationships (19) are obtained by using (A.2) and (18). Appealing to (**6**) the function W_2 thus reads

$$W_2 = c^2(\cosh\xi - \lambda)^{1/2} \sin^2\eta \sum_{n\geqslant 2} [A_n \sinh(\gamma_n\xi) + A'_n \cosh(\gamma_n\xi)]P''_n(\lambda) \tag{A.4}$$

with $\lambda = \cos\eta$ and Q_2, W_1 and W_3 given by (21b) to (21d). Because the velocity $\mathbf{u}$ vanishes on the plane wall $\xi = 0$, one requires that $A'_n = 0$ for $n \geqslant 2$ (since $u_z = 0$ and the pressure $\mu Q_2 \sin 2\phi$ is bounded for $\xi = 0$) and

$$[W_1]_{\xi=0} = [W_3]_{\xi=0} = -\left[\frac{\rho Q_2}{2c}\right]_{\xi=0}, \quad [Q_2]_{\xi=0} = -\lim_{\xi\to 0}\left[\frac{2W_2 c}{z}\right]. \tag{A.5}$$

Exploiting the identities (where primes again denote differentiation with respect to λ)

$$(2n+1)P''_n(\lambda) = P'''_{n+1}(\lambda) - P'''_{n-1}(\lambda), \tag{A.6a}$$

$$(2n+1)\lambda P''_n(\lambda) = (n+2)P''_{n-1}(\lambda) + (n-1)P''_{n+1}(\lambda) \quad \text{for } n \geqslant 1, \tag{A.6b}$$

$$(2n+1)(1-\lambda^2)P''_n(\lambda) = (n+1)(n+2)P'_{n-1}(\lambda) - n(n-1)P'_{n+1}(\lambda), \tag{A.6c}$$

it is easy to derive (22a), (22c) and the relationships (22f) for the coefficients B_n, D_n and F_n (the procedure is similar to the one employed by (**7**)). Let us now turn to the boundary condition (17) on the sphere surface $\xi = \alpha$. In our notation (17) becomes

$$[Q_2]_{\xi=\alpha} = -\left[\frac{2W_2 c}{z}\right]_{\xi=\alpha}, \quad [W_1]_{\xi=\alpha} - \frac{2\sinh\alpha\sin\eta}{(\cosh\alpha - \cos\eta)^2} = [W_3]_{\xi=\alpha} = -\left[\frac{\rho Q_2}{2c}\right]_{\xi=\alpha}. \tag{A.7}$$

Using again (A.6a) to (A.6c) in conjunction with the previously obtained formulae for B_n and F_n and the identity

$$\frac{\sinh\alpha}{(\cosh\alpha - \cos\eta)^2} = \frac{4\sqrt{2}}{3}(\cosh\alpha - \cos\eta)^{1/2} \sum_{n\geqslant 1}(n + \tfrac{1}{2})\mathrm{e}^{-(n+1/2)\alpha} P'_n(\cos\eta), \tag{A.8}$$

it is then straightforward to establish (22b), (22d) and (22f) for the coefficients C_n, E_n and G_n with definitions (23) of k_n and r_n. One finally needs to impose the divergence-free condition $\mathbf{\nabla}.\mathbf{u} = 0$ in the entire fluid domain, that is, for $0 \leqslant \phi \leqslant 2\pi, 0 \leqslant \eta \leqslant \pi$ and $0 \leqslant \xi \leqslant \alpha$. In our notation, this condition reads $T_1 + T_2 + T_3 + T_4 = 0$ with

$$T_1 = \frac{\partial W_1}{\partial \rho} - \frac{W_1}{\rho}, \quad T_2 = 3Q_2 + \rho \frac{\partial Q_2}{\partial \rho} + z\frac{\partial Q_2}{\partial z}, \quad T_3 = \frac{\partial W_3}{\partial \rho} + \frac{3W_3}{\rho}, \quad T_4 = 2\frac{\partial W_2}{\partial z}. \tag{A.9}$$

As can be immediately checked from the definition (20) of L^2_m, note that

$$\rho \frac{\partial}{\partial \rho}(L^2_m[g]) = L^2_m\left[\rho \frac{\partial g}{\partial \rho}\right] - 2L^2_m[g] + 2\frac{\partial^2 g}{\partial z^2}, \tag{A.10a}$$

$$z\frac{\partial}{\partial z}L^2_m[g] = L^2_m\left[z\frac{\partial g}{\partial z}\right] - 2\frac{\partial^2 g}{\partial z^2}, \tag{A.10b}$$

$$\frac{\partial}{\partial \rho}(L^2_m[g]) = L^2_m\left[\frac{\partial g}{\partial \rho}\right] + \frac{m^2 - n^2 - 1}{\rho^2}\frac{\partial g}{\partial \rho} + \frac{2n^2}{\rho^3}g, \tag{A.10c}$$

$$\frac{\partial}{\partial z}L^2_m[g] = L^2_m\left[\frac{\partial g}{\partial z}\right], \tag{A.10d}$$

$$\frac{1}{\rho}L^2_m[g] = L^2_m\left[\frac{g}{\rho}\right] + \frac{2}{\rho^2}\frac{\partial g}{\partial \rho} + \left[\frac{m^2 - n^2 - 1}{\rho^3}\right] g. \tag{A.10e}$$

Combining (20) and (A.10) successively for $(n, m) = (1, 2)$ and $(n, m) = (3, 2)$ it is then established that the functions T_1, T_2, T_3 and T_4 introduced by (A.9) obey

$$L^2_2[T_1] = L^2_2[T_2] = L^2_2[T_3] = L^2_2[T_4] = 0. \tag{A.11}$$

These identities prove (**6**) that each function T_i $(i = 1, \ldots, 4)$ admits the following form:

$$T_i(\xi, \eta) = (\cosh\xi - \cos\eta)^{1/2} \sin^2\eta \sum_{n \geqslant 2} [T^i_{s,n} \sinh(\gamma_n \xi) + T^i_{c,n} \cosh(\gamma_n \xi)] P''_n(\cos\eta). \tag{A.12}$$

Accordingly, the task consists in obtaining the above coefficients $T^i_{s,n}$ and $T^i_{c,n}$ in terms of the coefficients A_n, B_n, C_n, D_n, E_n, F_n and G_n by exploiting the definitions (A.9), the relations (A.6a) to (A.6c) and the additional identities

$$c\frac{\partial g}{\partial z} = (1 - \cosh\xi\cos\eta)\frac{\partial g}{\partial \xi} - \sinh\xi\sin\eta\frac{\partial g}{\partial \eta}, \tag{A.13a}$$

$$c\frac{\partial g}{\partial \rho} = -\sinh\xi\sin\eta\frac{\partial g}{\partial \xi} + (\cosh\xi\cos\eta - 1)\frac{\partial g}{\partial \eta}, \tag{A.13b}$$

$$(2n+1)(1-\lambda^2)P'''_n(\lambda) = (n-1)(2-n)P''_{n+1}(\lambda) + (n+2)(n+3)P''_{n-1}(\lambda), \tag{A.13c}$$

$$(1-\lambda^2)P'''_n(\lambda) = 6\lambda P'''_n(\lambda) - (n-2)(n+3)P''_n(\lambda). \tag{A.13d}$$

The procedure makes use of elementary algebra but the detailed calculations are too lengthy to be reproduced here. For a sake of conciseness, we content ourselves with giving the derived decomposition (A.12) for the

sum $T_1 + T_2 + T_3 + T_4$. Setting $T_{c,n} = \sum_{i=1}^{4} T^i_{c,n}$ and $T_{s,n} = \sum_{i=1}^{4} T^i_{s,n}$, the results, for $n \geqslant 2$, are

$$\frac{T_{c,n}}{c} = \frac{5}{2}B_n - \frac{n-2}{2}B_{n-1} + \frac{n+3}{2}B_{n+1} - \frac{D_{n-1}}{2} + D_n - \frac{D_{n+1}}{2}$$
$$- (n-2)(n+3)F_n + \frac{(n-2)(n-3)}{2}F_{n-1} + \frac{(n+3)(n+4)}{2}F_{n+1}$$
$$+ (2n+1)A_n - (n-2)A_{n-1} - (n+3)A_{n+1}, \tag{A.14a}$$

$$\frac{T_{s,n}}{c} = \frac{5}{2}C_n - \frac{n-2}{2}C_{n-1} + \frac{n+3}{2}C_{n+1} - \frac{E_{n-1}}{2} + E_n - \frac{E_{n+1}}{2}$$
$$- (n-2)(n+3)G_n + \frac{(n-2)(n-3)}{2}G_{n-1} + \frac{(n+3)(n+4)}{2}G_{n+1}. \tag{A.14b}$$

Of course, the divergence-free condition requires that $T_{c,n} = T_{s,n} = 0$ for $n \geqslant 2$. Using (22a), (22c) and (22f) it is easy to check that $T_{c,n}$ vanishes (this is due to the fact that the condition $\boldsymbol{\nabla}.\mathbf{u} = 0$ on the $\xi = 0$ plane Σ was already enforced when using (A.5)). Finally, applying the conditions $T_{s,n} = 0$ for $n \geqslant 2$ yields, by virtue of (A.14b), (22b), (22d) and (22f) for the coefficients G_n the announced system (24).

A.3 *Determination of the disturbed flow about a fixed sphere embedded in an unbounded quadratic flow*

In this Appendix we build the disturbed velocity, $z^2\mathbf{e}_x + \mathbf{u}$, about a stationary sphere immersed in the *unbounded* quadratic ambient flow $z^2\mathbf{e}_x$ by the singularity method. For convenience we use the vector $\boldsymbol{X}$ introduced in section 2 and denote here its components ($X_1 = X, X_2 = Y, X_3 = Z$) and $\chi = |\boldsymbol{X}|$. Setting $(\mathbf{e}_1, \mathbf{e}_2, \mathbf{e}_3) = (\mathbf{e}_x, \mathbf{e}_y, \mathbf{e}_z)$, using the decomposition

$$z^2\mathbf{e}_x = \mathbf{v}_0 + \mathbf{v}_1 + \mathbf{v}_2, \quad \mathbf{v}_0 = \ell^2\mathbf{e}_1, \quad \mathbf{v}_1 = 2\ell Z\mathbf{e}_1, \quad \mathbf{v}_2 = Z^2\mathbf{e}_1 \tag{A.15}$$

and invoking the linearity of the Stokes equations, the required velocity disturbance $\mathbf{u}$ reads $\mathbf{u} = \mathbf{u}_0 + \mathbf{u}_1 + \mathbf{u}_2$, where the perturbation flows $(\mathbf{u}_m, p_m)$ obey for $m = 0$, 1 or 2

$$\mu\boldsymbol{\nabla}^2\mathbf{u}_m = \boldsymbol{\nabla}p_m \text{ and } \boldsymbol{\nabla}.\mathbf{u}_m = 0 \quad \text{for } \chi > a, \tag{A.16a}$$

$$(\mathbf{u}_m, p_m) \to (\mathbf{0}, 0) \text{ as } \chi \to \infty, \quad \mathbf{u}_m = -\mathbf{v}_m \quad \text{at } \chi = a. \tag{A.16b}$$

Each velocity $\mathbf{u}_m$ is obtained by placing a few singularities at the sphere centre. We introduce here, by their Cartesian components $\mathcal{T}_{\alpha\beta}(\boldsymbol{X})$, $G^c_{\alpha\beta}(\boldsymbol{X})$, $D_{\alpha\beta}(\boldsymbol{X})$ and $G^{\mathrm{str}}_{\alpha\beta\gamma}(\boldsymbol{X})$, the Stokeslet, rotlet, potential dipole and stresslet tensors, respectively, as

$$\mathcal{T}_{\alpha\beta}(\boldsymbol{X}) = \frac{\delta_{\alpha\beta}}{\chi} + \frac{X_iX_j}{\chi^3}, \quad G^c_{\alpha\beta}(\boldsymbol{X}) = \frac{[\mathbf{e}_j \wedge \boldsymbol{X}]}{\chi^3}.\mathbf{e}_i, \tag{A.17}$$

$$D_{\alpha\beta}(\boldsymbol{X}) = \frac{3X_iX_j}{\chi^5} - \frac{\delta_{\alpha\beta}}{\chi^3}, \quad G^{\mathrm{str}}_{\alpha\beta\gamma}(\boldsymbol{X}) = \frac{3X_iX_jX_k}{\chi^5}. \tag{A.18}$$

with $\delta_{\alpha\beta}$ the usual Kronecker delta. Note that $\mathcal{T}$ is related to the Oseen tensor

$$T_{\alpha\beta}(\boldsymbol{r}) = \frac{1}{8\pi\mu}\left(\frac{\delta_{\alpha\beta}}{r} + \frac{r_\alpha r_\beta}{r^3}\right) \tag{A.19}$$

by $T = 1/(8\pi\mu)\,\mathcal{T}$.

As established in (**18**) and easily verified, the result $\mathbf{u} = \mathbf{u}_0 + \mathbf{u}_1 + \mathbf{u}_2$ follows with, under the usual tensor summation convention, the following formulae:

$$\mathbf{u}_0(\boldsymbol{X}) = -\frac{3a^2 l}{4}\left\{\mathcal{T}_{i1}(\boldsymbol{X}) - \frac{a^2}{3}D_{i1}(\boldsymbol{X})\right\}\mathbf{e}_i\,, \tag{A.20a}$$

$$\mathbf{u}_1(\boldsymbol{X}) = -la^3\left\{G^c_{i2}(\boldsymbol{X}) + \frac{5}{3}G^{\mathrm{str}}_{13i}(\boldsymbol{X}) + \frac{a^2}{3}\frac{\partial D_{13}}{\partial X_i}(\boldsymbol{X})\right\}\mathbf{e}_i\,, \tag{A.20b}$$

$$\mathbf{u}_2(\boldsymbol{X}) = \frac{a^3}{24}\left\{-6\mathcal{T}_{i1}(\boldsymbol{X}) + 4a^2\frac{\partial G^c_{i2}}{\partial X_3}(\boldsymbol{X}) - 7a^2\left[\frac{\partial G^{\mathrm{str}}_{13i}}{\partial X_3}(\boldsymbol{X}) + \frac{\partial^2 D_{i1}}{\partial {X_3}^2}(\boldsymbol{X})\right]\right\}\mathbf{e}_i\,. \tag{A.20c}$$